Winter 2022

Assessing the Effects of Instream Large Wood on Floodplain Aquifer Recharge and Storage at Indian Creek, Kittitas County, Washington, USA

Stephen Bartlett
Central Washington University, stephen.bartlett@cwu.edu

ASSESSING THE EFFECTS OF INSTREAM LARGE WOOD ON FLOODPLAIN AQUIFER RECHARGE AND STORAGE AT INDIAN CREEK, KITTITAS COUNTY, WASHINGTON, USA

A Thesis

Presented to

The Graduate Faculty

Central Washington University

In Partial Fulfillment

of the Requirements for the Degree

Master of Science

Geological Sciences

---

by

Stephen P. Bartlett

March 2022

CENTRAL WASHINGTON UNIVERSITY

Graduate Studies

We hereby approve the thesis of

Stephen P. Bartlett

Candidate for the degree of Master of Science

APPROVED FOR THE GRADUATE FACULTY

_____ _____
Dr. Lisa Ely, Committee Chair

_____ _____
Dr. Carey Gazis

_____ _____
Dr. Breanyn MacInnes

_____ _____
Dean of Graduate Studies

ABSTRACT

ASSESSING THE EFFECTS OF INSTREAM LARGE WOOD ON FLOODPLAIN AQUIFER RECHARGE AND STORAGE AT INDIAN CREEK, KITTITAS COUNTY, WASHINGTON, USA

by

Stephen P. Bartlett

March 2022

Numerous stream restoration projects in the Yakima River Basin in Washington have placed large wood (LW) into tributary channels. One intended effect is to divert water onto floodplains to increase groundwater (GW) recharge and seasonal storage in shallow alluvial aquifers during spring high flows with the intention of releasing GW into streams during the drier summer months. Large wood was emplaced in the Indian Creek tributary of the Teanaway River in Kittitas County, Washington beginning in 2016. Potential changes in the groundwater recharge in the adjacent floodplain before and after the LW installation were investigated through stratigraphic analysis, stream-flow modeling, and GW levels in six piezometers installed in 2014 and 2018. Stratigraphic descriptions of the stream banks reveal a ubiquitous silt/clay dominant layer (60-90 cm thick) at a depth of 1 meter or less, overlying a sand and gravel layer (15-50 cm thick), a clay/silt layer (~30 cm thick), and another sand and gravel layer. These relatively continuous clay layers extend at least 2.2 km upstream from the mouth of Indian Creek on both sides of the channel. Similar clay units have been mapped in the region as glacial drift or lacustrine deposits. The measured stream flow and GW levels in the monitoring wells before and after the LW emplacement show no detectable effect of the LW on

seasonal or longer-term GW levels. Data loggers show that GW levels return to baseflow within days of monthly precipitation exceeding 70 mm, suggesting GW flow within the permeable sand and gravel layers beneath or between the clay/silt layers. Available data show that the highest spring GW elevations precede peak stream discharge, indicating that the peak streamflow is not a significant source of GW recharge. A 1-dimensional hydraulic model run with and without channel obstructions at spring monthly average discharge and peak discharge suggests that the water surface elevation may increase ~10-50 cm within and upstream of LW. This assessment of stratigraphy coupled with GW data and stream-flow model can provide insight into the effectiveness of GW recharge from LW restoration projects in similar settings within the region.

ACKNOWLEDGMENTS

This research was funded through a grant from the Washington State Department of Ecology (IAA No C2100007) to C. Gazis and L. Ely as part of the Yakima Basin Integrated Plan. I would like to thank Carey Gazis and Lisa Ely for giving me the opportunity to work on this project and for all their efforts in making this project possible. I would also like to thank them for all their help and guidance throughout this process. I would like to thank my daughter, Lily, whose presence motivated me to choose this path, for helping me stay on track, and providing entertainment throughout this process.

TABLE OF CONTENTS

LIST OF TABLES

LIST OF FIGURES

LIST OF FIGURES (CONTINUED)

CHAPTER I

INTRODUCTION

Large wood (LW) was once a prominent feature found throughout many streams in the United States (Wohl, 2014). Removal of LW was a top priority for European settlers as they moved westward (Wohl, 2014). Reasons for the removal of LW included river navigation, flooding, timber floating, and to improve fish passage, among others (Reich et al., 2003, Maser and Sedell, 1994, Whitney, 1994). At present, ecosystems are showing the deteriorating effects of historical LW removal (Mellina and Hinch, 2009, Wohl, 2014).

Large wood removal has created a myriad of consequences to stream corridors and ecosystems. A few of these consequences include loss of aquatic and riparian habitats, and changes to channel morphology and hydrology (Swanson and Lienkaempber, 1978, Díez et al., 2000; Reich et al., 2003). Fish rely on the lower velocities and pools that LW help create within the channel (Dolloff and Warren, 2003). Many juvenile fish species and other living species use instream LW as shelter from environmental factors and predators (Nagayama et al., 2012; Jones et al., 2014; Enefalk et al., 2017).

Not only fauna, but flora is affected by the removal of instream LW. The loss of instream LW has reduced the density and diversity of riparian vegetation. Riparian vegetation requires the direct interaction between the aquatic and terrestrial environments (Swanson et al., 1982). When LW is removed from the stream channel, the area in which these interactions occur is reduced in both length and width throughout the stream

corridor from the loss of pools, floodplain inundation area, and decreased duration of surface and groundwater interaction (Fetherston et al., 1995; Wohl, 2013; Nash et al., 2020). The riparian environment narrows along the stream corridor as the morphology of the stream narrows.

The changes to channel morphology and hydrology that have occurred due to the historic LW removal are primary factors that have aided in the decline of habitat. Channel complexity is greatly reduced in first and second order streams without instream obstructions such as LW (Figure 1). Channel width decreases and channel incision increases as instream obstructions are reduced (Jackson and Sturm, 2002). As the stream channel becomes more simplified, the dynamics of the hydrology are reduced. Resistance caused by log jams that create upstream pooling, which aids in increasing surface water infiltration and subsurface flow, decreases and the stream water becomes disconnected from the floodplain (Tonina and Buffington, 2009; Wohl, 2013).

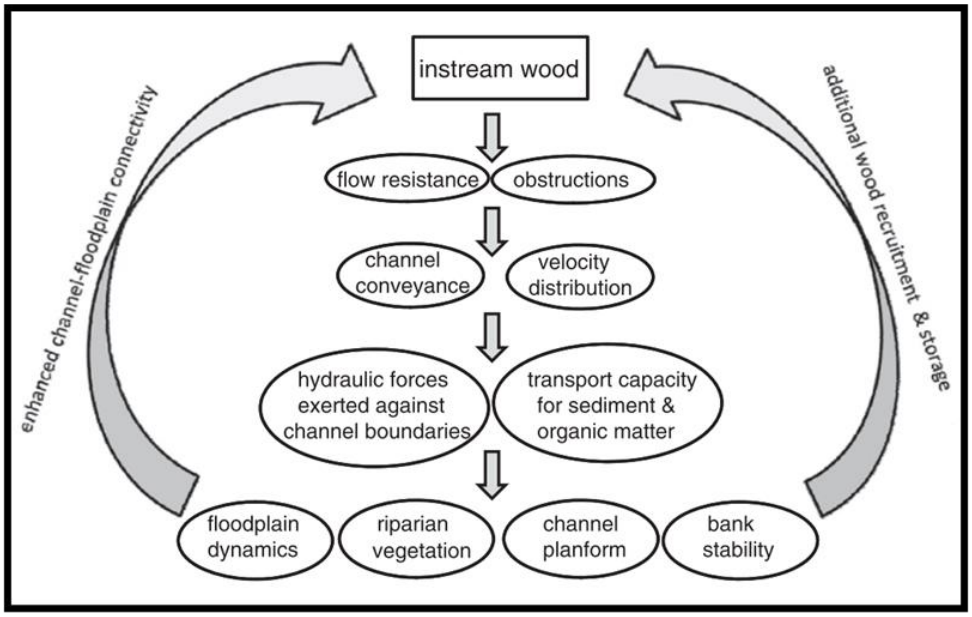

Figure 1. Instream wood diagram of the effects of instream wood on channel complexity from Wohl, (2013).

Project Purpose

Large wood restoration in streams has become a common method in attempting to restore the natural habitat. This type of restoration has become widespread within the Yakima Basin in Washington, USA (Figure 2) where many streams have undergone or are currently undergoing restoration. Over the past 30 years, many researchers have studied the effects the addition of large wood in the stream channel and floodplain have on geomorphic features and hyporheic exchange (Gurnell and Sweet, 1998; Sawyer and Cardenas, 2012; Wohl, 2013; Scott et al., 2019; Mao et al., 2020). There have been few studies looking at the effects of stream restoration on groundwater recharge and late season discharge. One reason for this gap in our knowledge is the lack of useful monitoring data available for restoration areas (Tague et al., 2008). The numerous LW restoration projects underway in the Yakima Basin present an opportunity to assess the effect that LW restoration has on storage and recharge of the shallow floodplain aquifers.

The purpose of this study is to assess the effects that instream LW restoration has on the recharge and storage of groundwater in the alluvial floodplain aquifer at Indian Creek in Kittitas County, Washington (Figure 2). This assessment involved the description of aquifer stratigraphy, the manual recording of groundwater levels and the analysis of groundwater levels from pressure transducers since 2014. It also included a one-dimensional streamflow model to investigate the possibility of increased floodplain inundation.

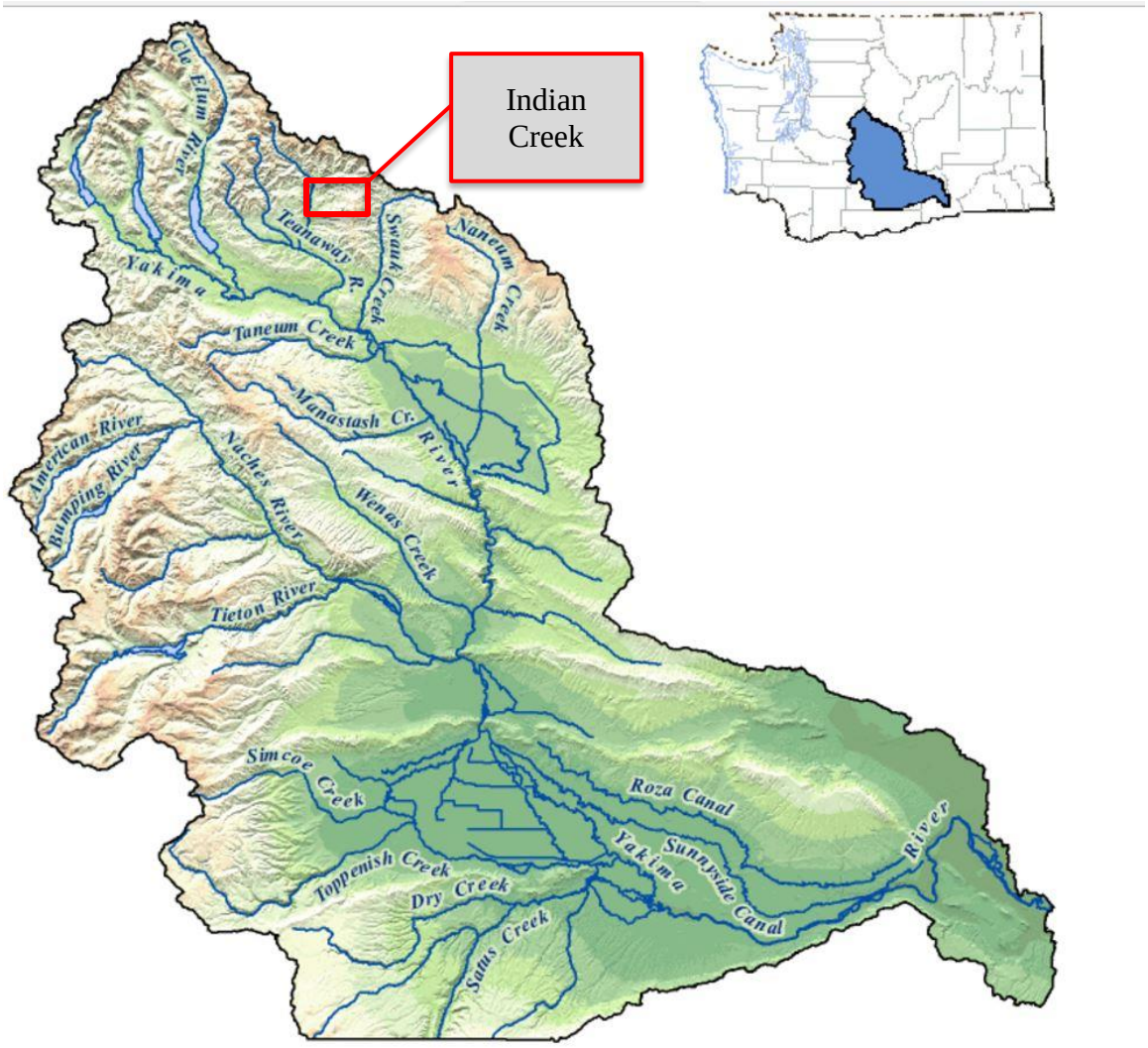

Figure 2. Yakima Basin watershed. Study area highlighted in red box. Image credit: https://ecology.wa.gov/Blog/Posts/April-2019/After-40-years,-Acquavella-adjudication-is-coming#gallery-3

Significance

Understanding how instream LW affects the geomorphic response of stream channels is fairly well understood. Other work has focused on how the addition of instream LW affects the hyporheic exchange of the stream immediately after emplacement (Sawyer and Cardenas, 2012). At this time, little is known about how soon after emplacement instream LW may affect floodplain GW recharge and storage (Emmons, 2013; Nash et al., 2020). This research aims to provide insight into the short-term effectiveness of instream LW restoration on floodplain GW recharge and storage at Indian Creek and settings similar to it.

Often, LW wood restoration projects are implemented with little understanding of the sedimentary composition of the adjacent aquifer. Understanding the hydrologic dynamics between the floodplain and stream in the region or setting can help project managers determine the sites where LW might increase the interaction between the surface water in the channel and the floodplain, and thus might be effective for GW recharge and storage. A recent study of the area by Boylan (2019) looked at the link between the wood restoration and aquifer recharge at Indian Creek. Boylan (2019) modeled GW flow in an aquifer of uniform composition and an assumed thickness. This study builds on the results from Boylan (2019) by investigating the interactions of the surface water and groundwater and how the stratigraphy of the aquifer affects the dynamics of the hydrology.

Yakima Basin Integrated Plan

The arid climate of eastern Washington coupled with the projected decrease in future snowpack in the Cascade Mountains (Gergel et al., 2017) makes the current water usage within the Yakima Basin unsustainable. Snowpack at elevations below 2000 m is the most susceptible to experiencing the effects of climate change (Sproles et al., 2013). Present water issues and the future projections meant mitigation efforts are warranted to sustain water resource use.

The Yakima Basin Integrated Plan (YBIP) is a diverse group of stakeholders who came together to work toward ensuring the future availability of water in the Yakima Basin. There are seven elements to accomplish the goals of the YBIP. The elements are reservoir fish passage, structural and operational changes, surface water storage, groundwater storage, habitat/watershed protection, enhanced water conservation, and market reallocation.

Indian Creek Large Wood Restoration

The Yakama Nation, a stakeholder in the YBIP, has conducted many LW restoration efforts. The primary purpose of the LW restoration is to restore aquatic habitat. A restoration project in the Teanaway Community Forest (TCF) (Figure 3) has recently been implemented in order to restore hydrologic and habitat function (DeKnikker, 2016). The project goal is to restore habitat for the improved production of Yakama Nation treaty reserved fish species (Deknikker, 2016). To improve fish habitat the LW wood is emplaced to reduce stream velocity, encourage deposition of sediment, and increase stream complexity.

The project at Indian Creek involved the placement of LW throughout the stream channel as well as the adjacent floodplain over an approximate 3-km stretch. Emplacement of the wood began in the summer of 2014, mostly on the floodplain. The installation of wood into the channel began in 2016 and has continued through 2021. The instream LW was placed in many large dense piles from near the mouth of Indian Creek to approximate 1.5 km upstream (Figure 4). Individual logs or small LW piles were placed in other areas of the stream or between areas of dense LW jams.

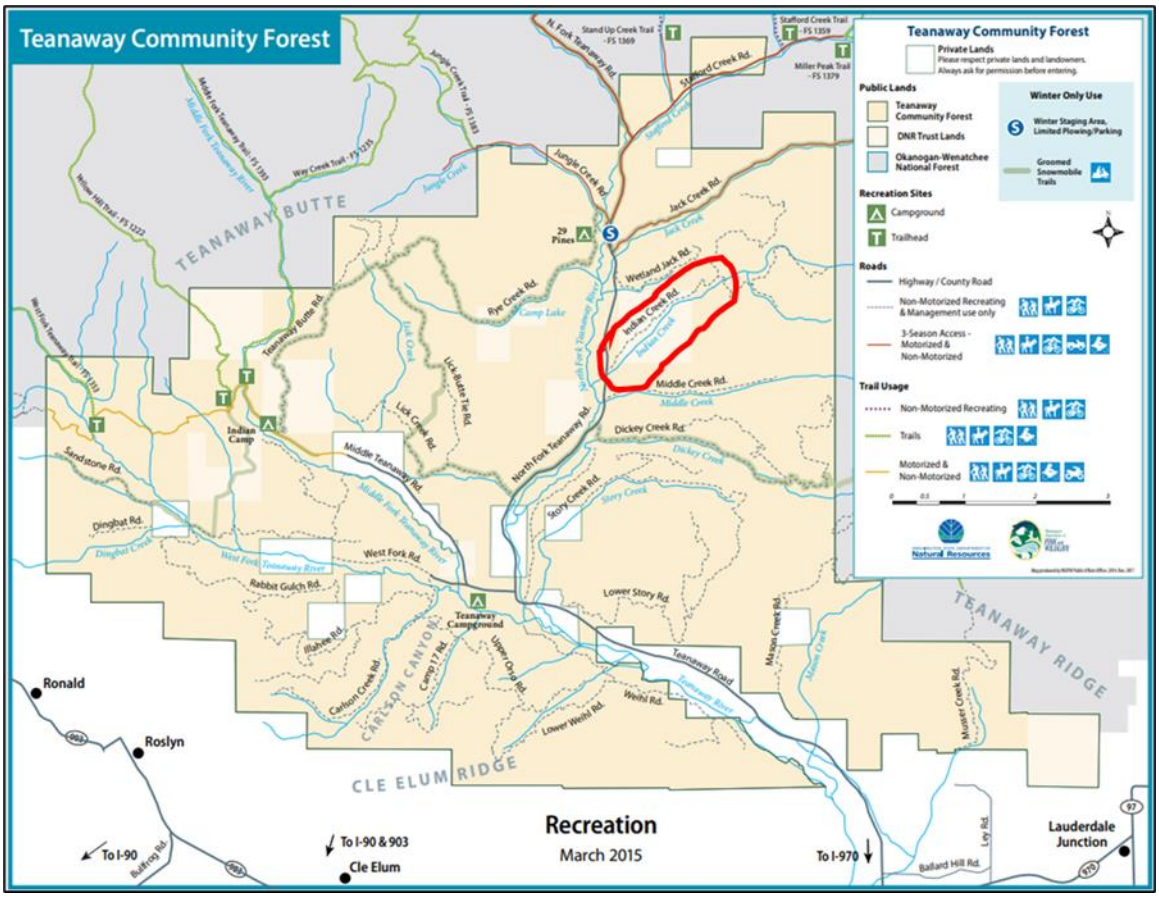

Figure 3. Map of the Teanaway Community Forest. Tan color is the Teanaway Community Forest. The location of Indian Creek is circled in red. Image from https://www.dnr.wa.gov/publications/amp_rec_tcf_map2015.pdf.

Figure 4. Aerial photo of instream large wood restoration of Indian Creek near North Fork Teanaway road just upstream from the DOE gauge (Figure 5A). (Image credit: Isaac Mitchell)

Geologic and Climatic Setting

Indian Creek is located near the base of the eastern side of the central Cascade Mountains. It is a tributary to the North Fork Teanaway River (NFTR) within the Yakima River basin (Figure 2). The upper elevations of the watershed are composed of the volcanic Teanaway Formation from approximately 50 million years ago (m.a.) (Tabor et al., 1984). The basin bedrock, and bedrock of Indian Creek is composed of the Roslyn Formation sandstone (47 m.a.) with stream corridors filled by Pleistocene glacial drift and outwash (Figure 6) (Eddy et al., 2017). The glacial drift and outwash deposits are characterized by poorly defined layers of boulders, pebbles, sand, silt, and lacustrine clay. Although the glacial lacustrine sediment is constrained to the lower reaches of the Teanaway River valley on the map (Figure 6), the lacustrine clay occurs in the floodplain stratigraphy farther up the Teanaway valley and its tributaries.

Most of the precipitation at Indian Creek falls between October and March (Prism Climate Group). Stream discharge rises rapidly in the early spring, usually peaking between early April and early May (Washington Department of Ecology stream gauge ID: 39T060). During the peak discharge, in areas where the creek banks are less than 40-cm high, water overtops the banks and flows out onto the floodplain (Figure 7). Discharge then rapidly subsides in early May. The stream bed is mostly dry by the middle of summer (Figure 8), excluding some stagnant ponds and some reaches of trickling flow (Figure 9).

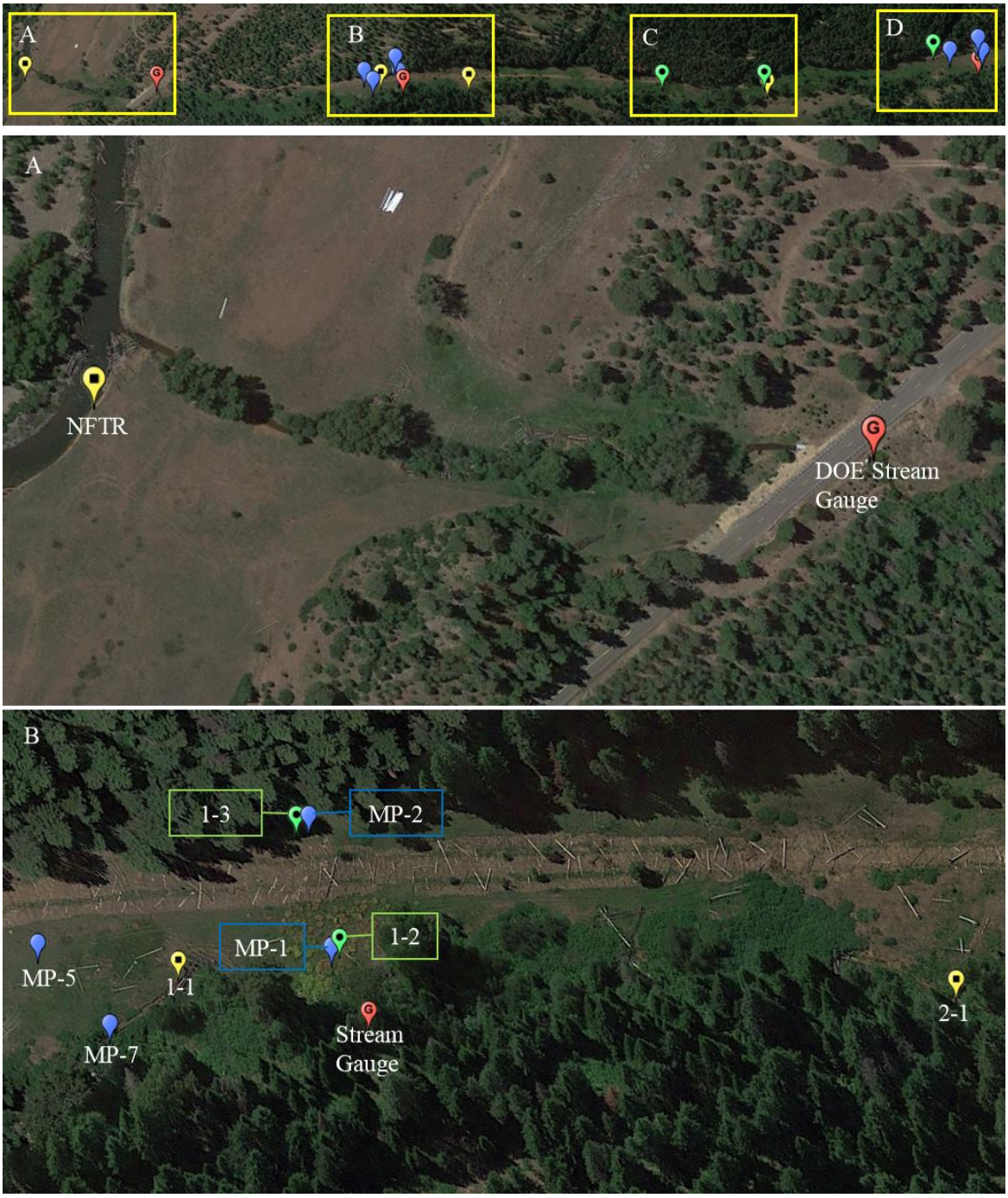
A
B
C
D
A
NFTR
DOE Stream
Gauge
B
1-3
MP-2
MP-1
1-2
MP-5
1-1
MP-7
Stream
Gauge
2-1

Figure 5. Study area of Indian Creek. Image A shows the downstream reach near the North Fork Teanaway River. Image B shows the downstream well cluster. Image C shows the middle reach. Image D shows the upstream reach and well cluster. Blue markers represent the groundwater monitoring wells. Green markers represent the floodplain stratigraphy sites. Yellow markers represent the stream bank stratigraphy sites. Red markers represent stream gauges.

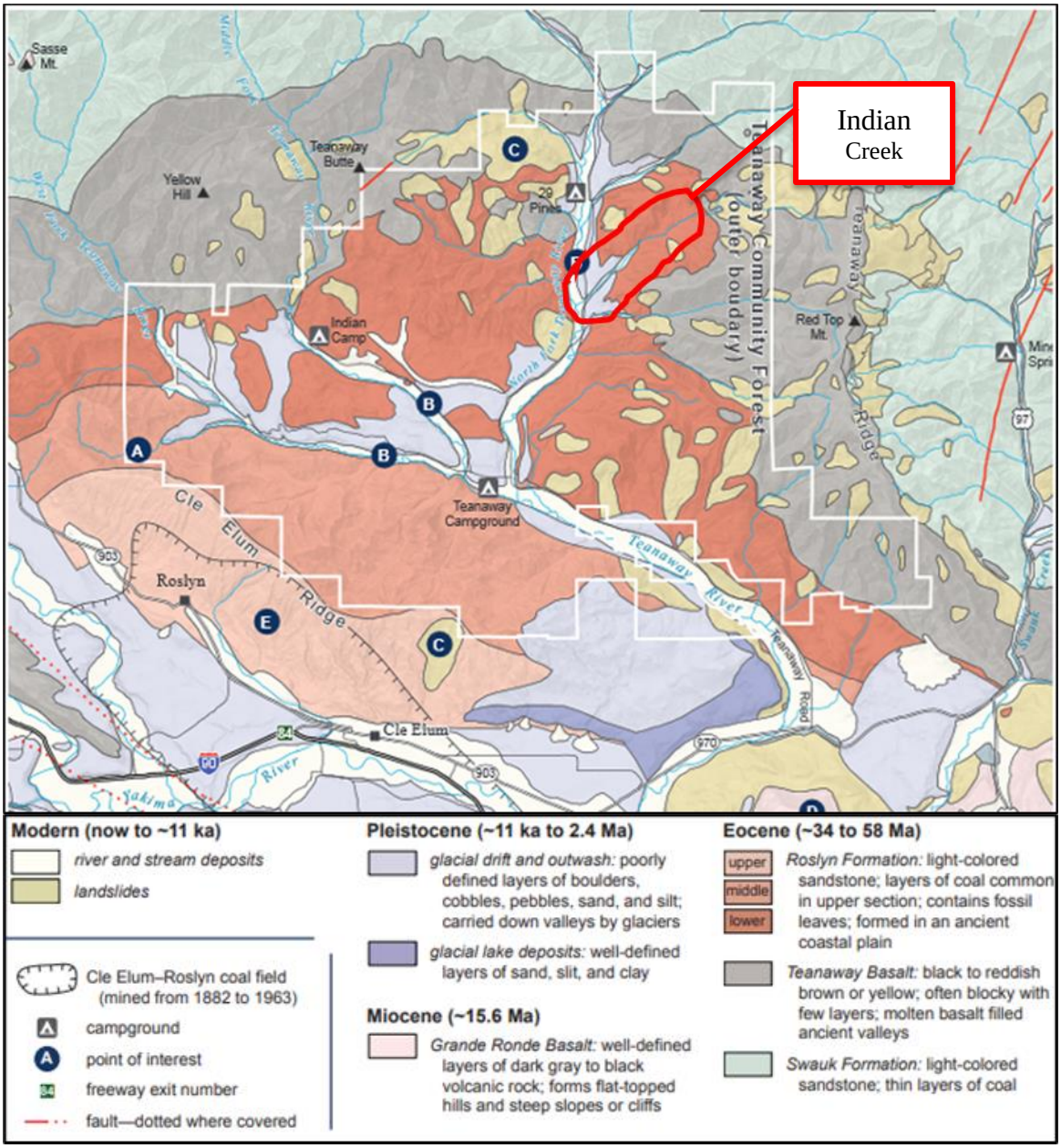

Figure 6. Geology of the Teanaway Community Forest by the Washington State Geological Survey. Map from Tabor et al. (1984).

Figure 7. Floodplain inundation of surface water during peak discharge. 04/17/2020. The floodplain just downstream of the gauge in Image C. Image by Stephen Bartlett

Figure 8. Dry stream channel at Indian Creek. Looking upstream at an instream large wood jam in the Indian Creek channel during summer. Located near the mouth of Indian Creek in Image A. Most of the stream channel is dry. 8/22/2020. Image by Stephen Bartlett

Figure 9. Photograph of Department of Ecology stream gauge. Stagnant water on 8/22/2020. Image by Stephen Bartlett

The floodplain of Indian Creek is equipped with six groundwater monitoring wells. Four wells were installed by the Washington Department of Natural Resources in 2013. Three more wells were installed in 2018 by Boylan (2019), however one of the wells (MP-7) is no longer present at the site. The wells that do exist are in two triangular configurations (Figure 5). They are located at 0.5 and 1.5 km upstream from the mouth of Indian Creek.

Boylan (2019) investigated the changes in groundwater level, flow direction, and gradients at the two well sites. No notable increase to the overall groundwater table was discovered at any of the wells in the study. Groundwater flow direction at the upstream well cluster was found to flow away from or parallel with the stream at different times. Direction of flow in the downstream well cluster was found to flow towards the stream. The groundwater gradient at the downstream wells was shown to increase toward the stream in the years following wood placement. At the upstream wells, the negative gradient between MP-3 and the stream was possibly reduced between 2014 and 2018. The gradient between MP-4, at the far edge of the floodplain near the hillslope, and the stream became more negative, and the direction of GW flow was therefore away from the stream. Although the gradient became less between the stream and MP-3, the gradient remains away from the stream.

CHAPTER II

METHODS

Groundwater and Stream Flow

Groundwater levels were documented using manual measurements and pressure transducers installed in each groundwater monitoring well (Table 1). Wells MP-1, 2, 3, and 4 are equipped with vanEssen Micro-Diver pressure transducers installed in 2014 by Kittitas Community Trust and Washington State Department of Ecology (DOE) (Boylan, 2019). The pressure transducers record measurements at 15-minute intervals. A barometric data logger of the same brand was placed hanging in a nearby tree at each of the two well clusters to compensate for atmospheric pressure.

Wells MP-5, 6, and 7 were installed October 26, 2018, by Boylan (2019). MP-5 is equipped with a MadgeTech Level1000s pressure transducer. MP-6 is equipped with a HOBO U20 Water Level Logger (Boylan, 2019). These data loggers collect a measurement every 15 minutes. MP-7 is no longer in existence on the floodplain of Indian Creek and was not present when this project began in the spring of 2020.

Table 1. Piezometer specifications of wells MP-1 through 6. Coordinates taken from Boylan (2019). Pressure transducer depths for MP-1,2, 4, and 5 taken from Boylan (2019). Below top of pipe.

Piezometer ID	Type	Latitude	Longitude	Piezometer Depth (m bTOP)	Transducer Depth (m bTOP)	Length of Pipe (m)
MP-1	3/4" OD steel	47.30491 N	120.84885 W	2.05	2.02	0.6035
MP-2	3/4" OD steel	47.30517 N	120.84930 W	2.83	2.72	0.201
MP-3	3/4" OD steel	47.31395 N	120.83617 W	1.48	1.40	0.552
MP-4	3/4" OD steel	47.31411 N	120.83648 W	2.89	2.82	0.12
MP-5	2" OD PVC	47.30438 N	120.84967 W	1.86	1.70	0.378
MP-6	2" OD PVC	47.31353 N	120.84925 W	2.59	2.46	0.643

Groundwater level data for 2014 to 2018 were obtained from Boylan (2019). Pressure transducer data beyond 6/18/2019 were downloaded and processed by the Central Washington University Geological Sciences Department. Manual groundwater level data from 10/27/2018 to 4/4/2019 were obtained from Boylan (2019).

Pressure transducer data were compensated with atmospheric pressure to produce a pressure head in centimeters. The pressure transducer immersed in water records the changes in total pressure, water pressure plus atmospheric pressure. Atmospheric pressure is measured by a transducer placed above ground in the area. Atmospheric pressure is then subtracted from the total pressure recorded by the immersed devices to get the change in relative water pressure. The relative water pressure is then converted into water depth.

Manual groundwater levels beginning 6/28/2020 were taken using an electronic water level tape that measures depth to groundwater. Depth to GW was recorded in feet,

and later converted to meters, from the top of the well pipe.

Water levels for the pressure transducer data and manual measurements were converted to elevation above mean sea level (m a.m.s.l) in meters. Manual measurements were converted using the following equation:

$$Ew = Es - (df)\ (0.3048) + p$$

Where Ew is the water elevation above sea level in meters; Es is the surface elevation of the well obtained from the topographic survey; df is the depth to water from top of pipe, in feet; and p is the length of the pipe above ground.

Upon downloading data from pressure transducers, several problems with the data became apparent. Data from MP-1 acquired from Boylan (2019) and recent data had a continuous downward drift that dropped readings to levels below the pressure transducer. The data were plotted on an elevation vs. time graph. The slope was numerically adjusted in Microsoft Excel to create a horizontal trend. When the prior data from Boylan (2019) and the recent data were graphed together a 0.22597 m difference existed between the datasets. To adjust this difference, 0.22597 m was subtracted from the data between 6/12/2014 to 5/21/2018.

Recent data from MP-2 showed a malfunction with the pressure transducer. The device did not record changes in pressure beyond 6/18/2019, rendering all readings after that period unusable. The cable holding the pressure transducer in well MP-3 corroded and broke on 7/2/2020; the transducer fell to the bottom of the well and is irretrievable. It was replaced near the end of this study, but no new pressure transducer data has been retrieved since 7/2/2020. Because of these problems much of the recent data relies on

manual measurements.

Ground Survey

A Topcon Real Time Kinematic (RTK) Global Positioning System was used to obtain elevation and position data. The RTK system consists of a stationary base station and a rover device. Each device communicates with multiple satellites as well as each other. The rover is set up at each desired location, given some time to locate its position using the satellites, then the point is recorded using a handheld tablet.

For the first trip, the base station was placed in an open field just west of MP-5 (Figure 5). Each monitoring well, stratigraphic column site, and Washington Department of Ecology (DOE) stream gauge were surveyed for position and elevation. The Washington Department of Natural Resources (DNR) section corner monument T21N R16E located downstream/west of MP-5 was also surveyed. Due to incomplete and inconsistent data at the upstream monitoring wells, surveying was performed a second time. The second base station position was farther upstream at a higher elevation near the road that runs the length of the area.

Due to elevation deviations exceeding three meters for some points collected by the RTK it was necessary to use a transit level to obtain more precise relative elevations of the groundwater monitoring wells within each cluster. The transit level consists of a stationary tripod that holds a monocular sight. Crosshairs are used to pinpoint the level on a measuring staff. The tripod was set up in a central location in each of the two triangular well clusters.

To adjust the elevations according to the transit level data, an elevation reference

point from the RTK data was chosen at each well cluster. The elevation of MP-6 was used as reference for the upstream well cluster. The elevation for MP-5 was used as reference for the downstream well cluster and the DNR section corner. These two points were chosen as reference elevations because they had the smallest standard deviation, 0.007 m or less.

Using the reference elevations, the elevation of the tripod location was determined by subtracting the staff reading from the height of the tripod and adding the difference to the reference elevation. The following equation was then used to calculate the adjusted elevations.

$$(h-P)/100 + R = PE$$

Where PE is the elevation of the point of interest, h = the height of the base, R is the reference point elevation and P is the reading taken by the transit level, and 100 is to convert centimeters to meters.

Stratigraphy

The stratigraphy of the aquifer was described at three banks along Indian Creek and one bank of the NFTR near the mouth of Indian Creek (Figure 5). Six locations throughout the floodplain were also described using an auger (Figure 5). These locations were determined based on proximity to the groundwater well clusters and height of the stream bank. Sites 3-1, 3-2, and 4-1 were chosen as intermediate sites between the well clusters.

A 7.5-cm diameter auger bucket was used for the excavation. The auger excavations were continued until they reached a depth at which groundwater or cobbles

would no longer allow further excavation. Three of the floodplain stratigraphy sites (named MP-1, MP-1, MP-3) were described within three meters of wells MP-1, 2, and 3 (Figure 5). Site 3-2 is in an open, flat area approximately 500 meters downstream of the upstream well cluster and on the floodplain near site 3-1 (Figure 5-A). Site 4-1 is near a stream gage approximately 650 meters upstream of the downstream well cluster (Figure 5-A). 4-1 was in a surface depression approximately two meters from the stream bank.

Stream bank sites were chosen based on height of exposure, accessibility, and relevance to the study area. Bank descriptions were a minimum of 2 meters from surface to stream bed. They provided a comfortable work area that was easy to access where mobility was not a problem. All stratigraphy sites at Indian Creek are located at or between the two well clusters (Figure 5). The work was performed in the months of July and August when the ground was relatively dry, and the stream stage was near its minimum.

The two-meter-tall banks, labeled as 1-1, 2-1, 3-1, and North Fork Teanaway River (NFTR) (Figure 5), provided exceptional areas of exposed stratigraphy. The stream bank column was measured by draping a long measuring tape from the surface down to the stream bed. Using a diamond-shaped hand trowel, a transplanting shovel, and a World War 2 folding shovel, the surface layer was carefully scraped away to freshen the sediment and expose clean contacts between stratigraphic units. Characteristics described during analysis were sediment color using a Munsell color chart, grain size, mottling, presence of roots, and oxidized rhizomes. Contacts between stratigraphic units were determined by changes in sediment size and/or consolidation. These changes included

deposition of gravels with an increase in sand or the decrease in coarse-grained sediment with abrupt increases in fine-grained sediment. These units were grouped into larger zones of similar sediment characteristics for stratigraphic interpretation. Sediment samples were collected from each zone for grain-size analysis.

Sediment Analysis

Sediment samples from stream bank site 1-1 (Figure 5) were used for grain-size analysis. This site was chosen because the strata identified there were found to be common throughout the stream banks and provide a general interpretation. At least one sample was collected from each identified stratigraphic zone. Multiple samples were taken from zones that contained enough variation throughout their thickness to warrant the extra analysis of the units within. All samples were analyzed using sieves and the Mastersizer 3000 LV for comparison.

Before processing of the sediment, all samples were dried in an oven at 100˚ C for 24 hours. The entire mass of each sample was then crushed using a pestle and mortar to eliminate or reduce consolidated clumps of fine-grained sediment. The full samples were weighed prior to being placed in the sieves. The mass retained in each sieve was weighed and recorded. Sieve sizes used were 4, 2, 1, 0.5, 0.25, 0.125, 0.063, 0.045 and 0.032mm. Sediment that sieved through 0.032 mm was weighed and labeled as <0.032 mm.

The fine-grained component of all samples was analyzed in the Mastersizer 3000 LV. Samples were first weighed, then sieved through a 0.5 mm screen. After the sieving, the mass retained and passed was recorded. The mass of the sample to be used in the

Mastersizer was determined by the Standard Operating Procedure for fine sediment. These amounts ranged from 0.10 to 0.13 g. The samples were placed in vials in a 30 ml of solution of water and sodium hexametaphosphate and mixed at a ratio of 5.5g/L to disperse flocculated clay and silt particles. The vials were shaken for 2 minutes and left to sit for 24 hours prior to analysis.

The Mastersizer 3000 LV performs three analyses per run. Each sample was run three times, yielding nine total analyses per sample. The nine outputs were averaged. The sample from unit 6 was run four times due to erroneous readings during the first run. Those data were not calculated into the average grain size. The outputs used were the d10, d50, and d90.

Porosity

Porosity of the aquifer is needed to determine potential storage capacity. To obtain an estimate of porosity values of the nine stratigraphic units identified within site 1-1, the sieve data were input to the HydrogeosieveXL program created by Devlin (2015). HydrogeosieveXL computes aquifer properties such as porosity, grain size analysis and 14 methods for determining hydraulic conductivity. HydrgeosieveXL does not accurately portray measurements of fine sediments and thus an error is involved in the porosity measurements.

Samples 5, 6, and 9 contain little to no coarse sediment grains, so porosity values were derived from the values determined by Schwartz and Zhang (2003). To estimate these values, the mass percent of sediment smaller than 0.063 mm per sample were summed. This percentage was used for the estimation of porosity by determining the

value associated with the corresponding percentage within the porosity range of silt and clay (Appendix C).

Streamflow Model

The Army Corps of Engineers Hydrologic Engineering Center River Analysis Systems 5.0.7 (HEC-RAS) was used to model the possible effects of the addition of large wood jams in the stream channel. HEC-RAS was used to model multiple discharges through a short example reach of the channel of Indian Creek where wood has been placed. This was to gain insight into what effect the addition of the wood has on the stage and velocity of the stream.

Discharges used in the HEC-RAS model were 6.0, 13.4, 15.9, and 36.4 ft^3/s. These discharges are average high discharge for the months of March, April, May, and the highest recorded discharge since 2014, respectively. Each discharge was run without obstructions and then run with in-channel obstructions. The scenarios were run using the "steady flow analysis" tool. Manning's 'n' hydraulic roughness values were set to 0.03 for the model without obstructions and 0.06 for the model with obstructions. Manning's 'n' hydraulic roughness values were determined using the 'USGS Guide for Selecting Manning's Roughness Coefficients for Natural Channels and Floodplains (Freeman et al., 1998).

Lidar imagery was used in the RAS-Mapper to determine the location of the stream channel. Teanaway bathymetry from 2015 was obtained from the Washington State Department of Natural Resources (DNR) Lidar Portal. Lidar for the area was collected prior to the placement of wood in the modeled reach. Because wood was not in

the stream at the time the Lidar was collected, it allowed for the model comparison to be done by adding virtual obstructions in the numerical model of the stream channel.

Using the HEC-RAS mapper tool, an approximately 1,040-foot channel profile was drawn down the middle of the current stream channel. This section was chosen because it is the area where the majority of the large wood was placed into the stream channel (Figure 4). Cross sections were generated automatically at a distance of 100 feet apart, beginning 115 feet upstream of the bottom of the modeled reach, and 100 feet wide. This procedure produced 13 cross-sections along the reach from 100 to 1300 feet up the reach. The cross section generating tool was used because it evenly places cross sections with the channel directly in the middle.

Using the “add obstructions” tool in HEC-RAS geometry editor, obstructions were placed throughout the channel of each cross section based on where the wood was observed on the 2019 drone imagery (Figure 4). Obstructions were placed only in the stream channel based on the presence of wood according to what is visible in the aerial imagery. The tool builds vertical obstructions at the desired width. The density of obstructions placed within each cross-section was chosen based on the results from Spreitzer et al., (2020), which showed a common average porosity of large wood jams to be approximately 66%. To simulate the density of wood piles, the obstructions were built as vertical blocks of varying height and thickness until the channel reached an approximate fill of 33%.

CHAPTER III

RESULTS

Ground Survey

Position data are from the RTK (Table 2). Elevation data of the well clusters were adjusted relative to a reference elevation in each well cluster using a transit level. The reference elevations were MP-5 in the downstream cluster and MP-6 in the upstream cluster. Locations of each point are in Figure 5. Points other than the reference elevations that do not have adjusted elevations were not surveyed with the transit level, so no adjustment is possible.

Table 2. Ground survey results. Positions based on surface elevations from the RTK data. *Elevations represent the reference elevations from the RTK data used for the adjusted surface elevations for the other wells in the clusters. Site locations in Figure 5.

Point	Northing	Easting	RTK Elevation	Adjusted Elevation
Section Corr	5241096.613	662425.501	736.614	736.714
MP-1	5241289.986	662598.678	742.795	742.992
MP-2	5241311.598	662576.512	746.884	742.627
MP-3	5242327.818	663531.568	780.843	781.682
MP-4	5242341.372	663508.562	782.037	782.01
MP-5	5241238.905	662544.086	740.772*	740.772*
MP-6	5242279.114	663477.186	779.81*	779.81*
1-1	5241259.52	662578.653	744.926	742.168
3-1	5241919.069	663242.895	769.728	
3-2	5241930.324	663222.017	769.961	
4-1	5241736.848	663045.2	758.127	
5-1	5242257.372	663439.567	779.68	
DOE Gauge	5240851.958	662192.8540	729.412	
Upstream Ga	5242302.381	663529.6610	784.635	780.429

Groundwater

Groundwater Elevations

Groundwater levels from pressure transducer data were converted to elevation above mean sea level (a.m.s.l) based on the adjusted RTK elevations of the ground surface at each well. Manual measurements obtained from Boylan (2019) and those obtained during this research period are shown in elevation a.m.s.l. (Table 3). Precipitation data were obtained for the region from the Oregon State University Prism Climate Group and is graphed with the groundwater elevation graphs for comparison (Figures 10 and 11). Stream discharge data were obtained from the DOE stream gauge data.

Table 3. Groundwater manual measurements from the six monitoring wells converted to elevation in meters a.m.s.l. Measurements taken before 2020 were taken by Boylan (2019). Original manual measurement data recorded in feet below top of well pipe is in Appendix A.

	MP-1	MP-2	MP-3	MP-4	MP-5	MP-6
10/8/2018	Dry	740.88	781.02	779.74	739.35	778.93
10/26/2018	Dry	741.31	780.89	780.26	739.42	778.87
4/4/2019	Dry	742.30	781.48	780.52	740.15	779.35
6/28/2020	Dry	741.05	781.04	779.77	739.30	778.87
8/26/2020	Dry	740.97	780.89	779.66	Dry	778.74
10/21/2020	Dry	741.09	781.27	779.87	739.30	778.88
4/11/2021	741.80	741.74	781.35	780.44	740.08	779.34
4/28/2021	741.63	741.30	781.34	780.35	739.65	779.30
5/9/2021	741.56	741.25	781.28	780.19	739.58	779.20
5/29/2021	741.54	741.13	781.17	779.97	739.30	779.02
6/10/2021	Dry	741.11	781.12	779.88	739.29	778.95
10/31/2021	Dry	741.14			739.33	
11/7/2021			781.12	779.33		779.02

Downstream Well Cluster

MP-1 pressure transducer data provide the clearest and longest signal of the water level (Figure 10). MP-1 goes dry every year in the spring and remains dry until late autumn or early winter (Table 4). Based primarily on MP-1, which is the closest well to the restoration area of the stream, pressure transducer data show the groundwater levels increasing from October-January. Groundwater usually increases from the annual low as the autumn precipitation arrives or when snow melt occurs (Table 4). The groundwater then rapidly decreases when the surface snow cover is nearly gone.

Some of the pressure transducer data depict times when the water level appears to drop below the depth of the pressure transducer and the bottom of the well, which is not possible. This apparent effect could be due to times when the water around the device freezes or some other temporary malfunction in the pressure transducer. A similar effect occurred in April 2020 and returned to a stable level in August 2020. A rapid jump occurs in the June 28, 2020, during which the pressure transducer was removed from the well and was returned August 26. The manual measurements from these dates show there was no change in water level during the time the device was not present.

Pressure transducer data and manual measurements from MP-2 show the groundwater level increase from and return to base level at approximately the same time as MP-1 (Figure 10). According to pressure transducer data and all manual measurements taken, MP-2 does not appear to go dry at any time throughout the year, and at base level the water remains about 1.5 meters above the bottom of the well. Visible in the MP-2 pressure transducer data are times of erratic readings. In the winter of 2016, the water

level appears to increase above the surface elevation of the well. During spring of 2017, the data drops suddenly. Data beyond the spring of 2017 is likely unreliable and is the probable point of device malfunction. Manual measurements show the groundwater elevation is often lower than the readings from the pressure transducer except shortly after its installation.

MP-5 pressure transducer data is minimal. No readings were recorded during the 2018 water year. The manual measurements taken by Boylan (2019) around the time of installation show a water-level increase, but there was no reaction from the pressure transducer. In January 2020 the water can be seen to increase rapidly with an increase in precipitation. Manual measurements then show it near base level in May. Problems occurred in the downloading of data after January 2020.

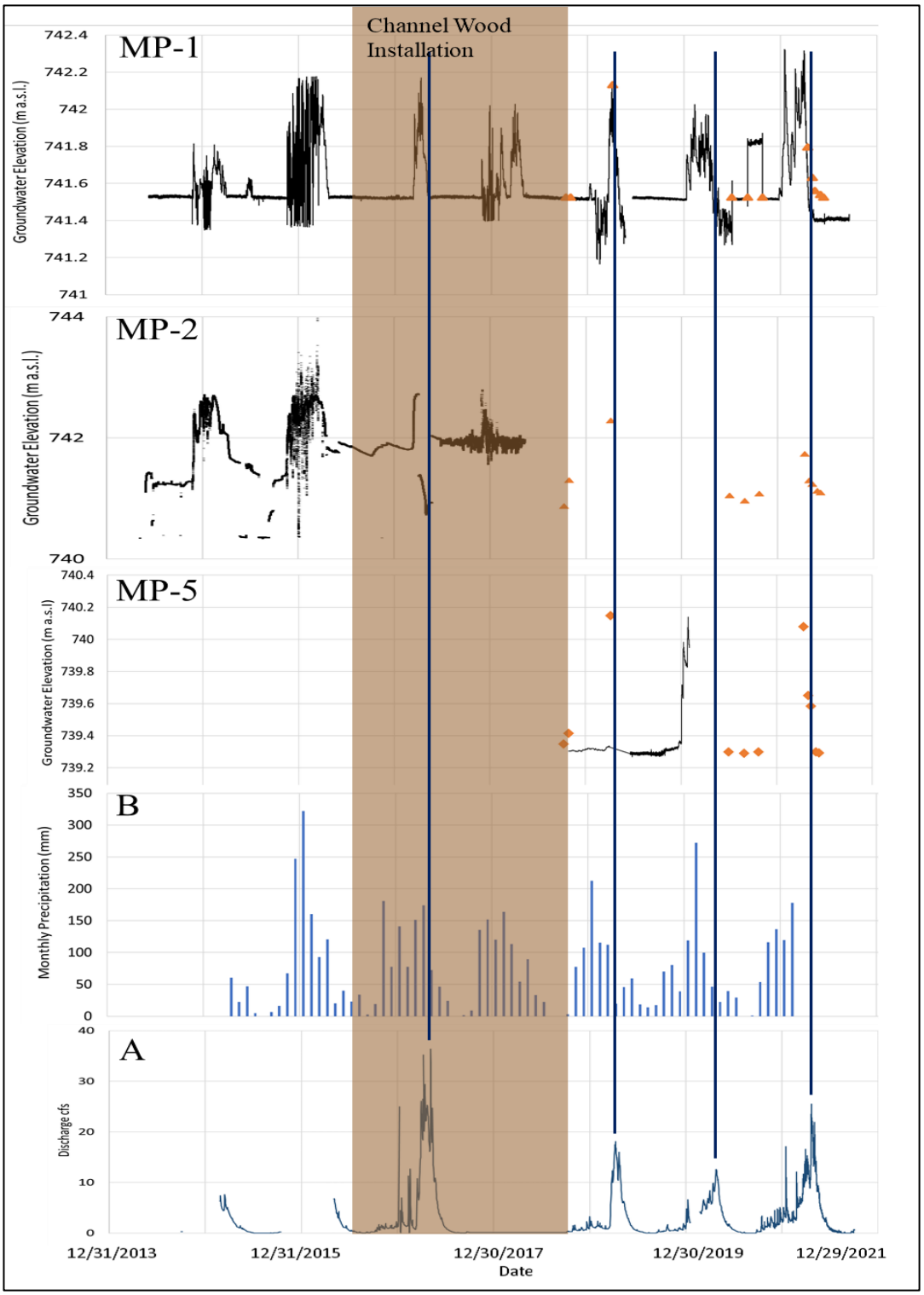

Figure 10. Pressure transducer data of the downstream well cluster compared to the stream discharge data (A) and the monthly regional precipitation data (B). Vertical brown shading represents the timeframe of wood installation. Vertical blue lines represent peak annual stream discharge. Orange diamonds represent manual measurements.

Table 4. MP-1 Wet/Dry dates. Dates MP-1 increased from dry, peaked, and returned to dry. * Date for 2020-2021 is a manual measurement and does not accurately reflect the date MP-1 went dry. The well was nearly dry when the previous manual measurement was taken on 5/29/2021 and was likely dry within a couple days.

MP-1	Wet	Peak	Dry	Days Wet
2014-2015	11/24/2014	11/29/2014	4/10/2015	137
2015-2016	11/17/2015	3/2/2016	4/29/2016	164
2016-2017	3/10/2017	4/7/2017	5/19/2017	69
2017-2018	11/23/2017	3/30/2018	5/13/2018	171
2018-2019	3/18/2019	4/4/2019	4/29/2019	42
2019-2020	1/7/2020	2/8/2020	4/17/2020	101
2020-2021	12/23/2020	1/14/2021	*6/10/2021	*169

Upstream Well Cluster

The pressure transducer data for the water levels in the upstream wells show dissimilar patterns from one another. In the 2015-16 water year the water level in MP-3 began to increase from base level in early December 2015 (Figure 11). It then returned to base level by mid-March 2016. In that same year, pressure transducer data for MP-4 showed the water level increasing in early January 2016 (Figure 11). The water then gradually declined, returning to a base level sometime in October 2016.

The MP-3 pressure transducer may have malfunctioned during the 2017 water year. The data show no change to water level in the spring of 2017. The MP-3 water elevation then increased by approximately 0.5 meters to 781.75 m a.m.s.l. in the spring of 2018. All data for MP-3 was obtained by Boylan (2019). The cable for the pressure transducer broke and the device is not retrievable. Excluding the instantaneous spikes in MP-3, a background level in the graphed data shows the accurate water level. The data appear to show an overall increase in water level from the beginning of recording, as was

mentioned by Boylan (2019). However, later manual measurements contradict such an increase to the base level GW and show the recent GW level to be consistent with the earlier base level readings from the pressure transducer.

MP-4 data show the water level increasing in March 2017 and declining to base level in October. The 2020 water year shows a clear increase to a peak water elevation of 781.1 m a.m.s.l. with a rapid return to base level by July. The accurate elevation for this period is the 8/26/2020 manual measurement at 779.65 m a.m.s.l. (Table 3).

A comparison of GW elevations with stream discharge and monthly regional precipitation shows GW levels commonly increase with increases in precipitation (Figure 10 & 11). The data also show the GW levels are commonly in decline prior to peak stream discharge. In the spring of 2017, MP-1 was nearly dry by the time of the stream peak discharge (Table 4).

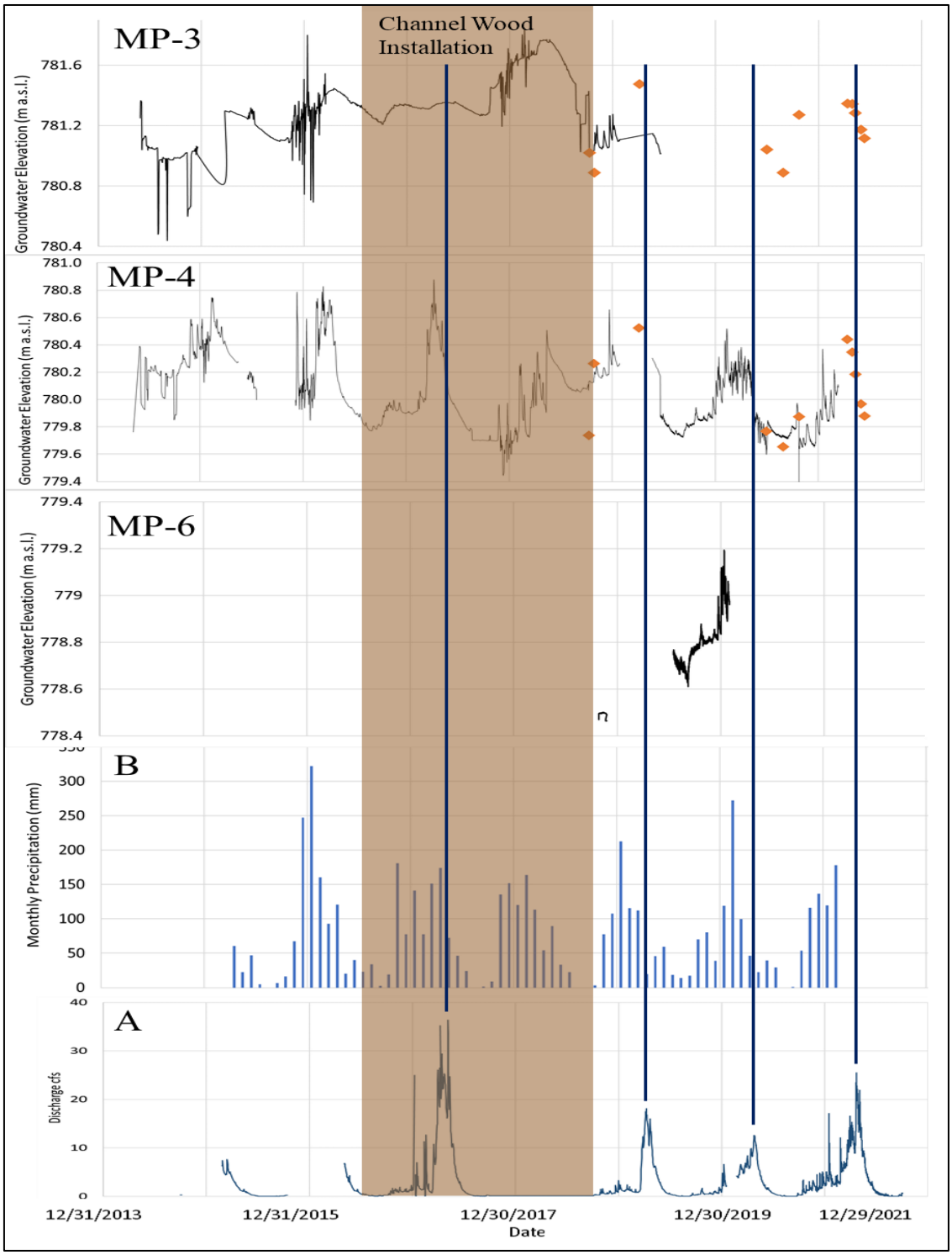

Figure 11. Pressure transducer data of the upstream well cluster compared to the stream discharge date (A) and the monthly regional discharge data (B). Vertical brown shading represents the timeframe of wood installation. Vertical blue lines represent peak stream discharge. Orange diamonds represent manual measurements.

The manual measurements capture the precise water elevation on the day taken (Figure 12 & 13). They are useful for comparing to the pressure transducers. The measurements taken in the spring of 2021 capture the decline in water level in all of the wells. The manual measurements also show nearly identical timing of water levels increasing and decreasing in all of the wells (Figure 14).

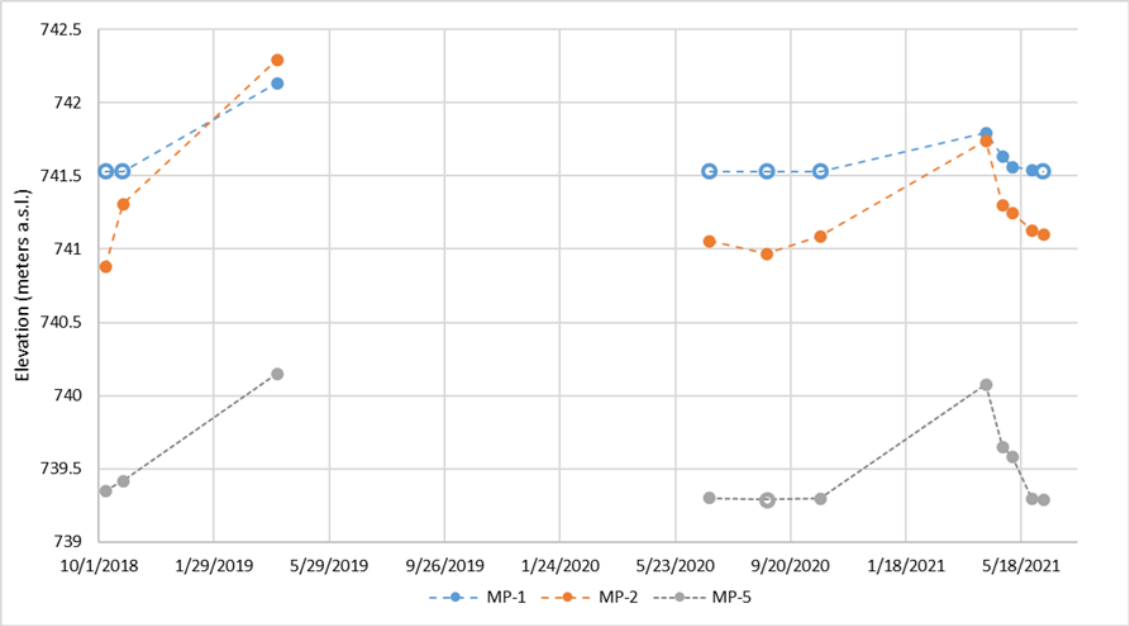

Figure 12. Manual measurements from the downstream well cluster. Measurements taken before 2020 were taken from Boylan (2019). Open circles represent a dry well.

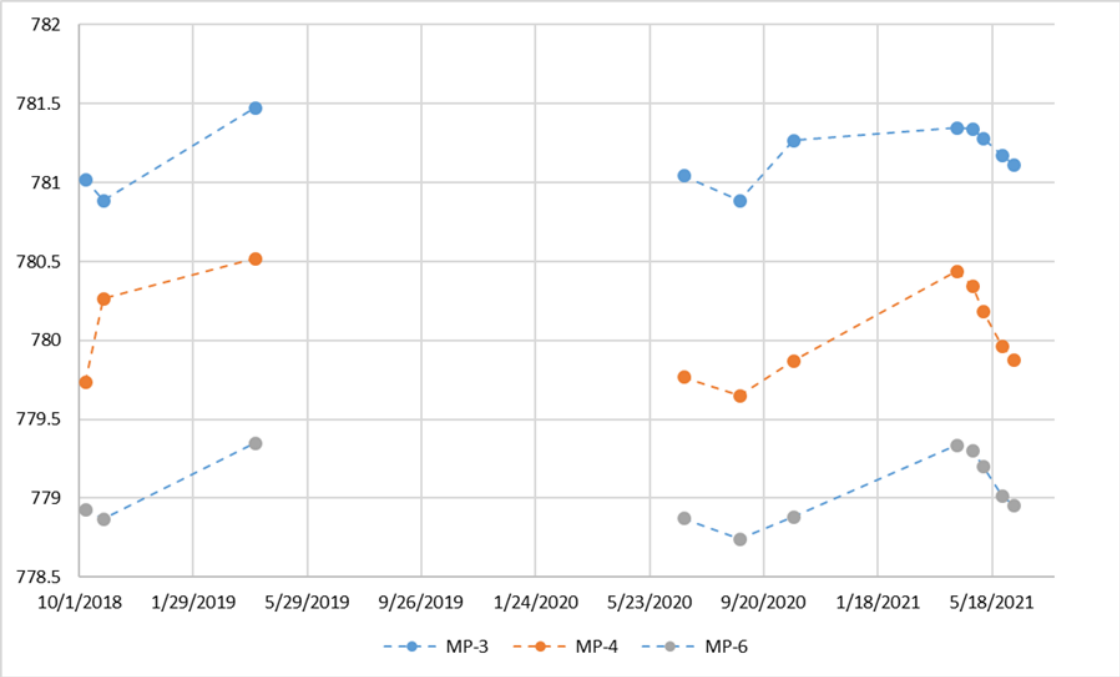

Figure 13. Manual measurements from the downstream well cluster. Measurements taken before 2020 were taken by Boylan (2019).

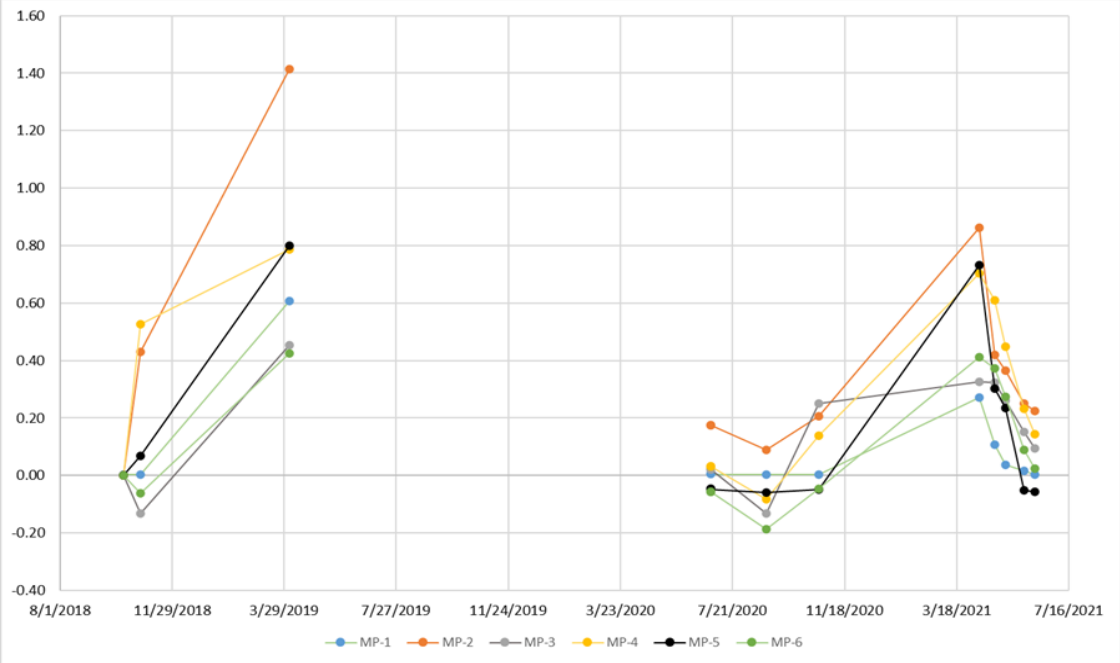

Figure 14. Comparison manual measurements from the upstream and downstream well clusters. The first measurement, dated 10/08/2018, has been set to 0. Measurements prior to 2020 were taken by Boylan (2019).

Stratigraphy

Stream Bank

The stratigraphic sites described from the NFTR bank near the mouth of Indian Creek to 1.4 km upstream of Indian Creek are remarkably similar (Figure 15). Each site is characterized by well-defined zones of silt, silt/clay, sand/silt/gravel, clay/silt, and gray clay (Figure 15). Some of zones contain multiple units differentiated by varying characteristics based on sediment composition and coloration. The thickness of the zones varies throughout the sites and are not continuous between sites 2-1 and 3-1. Each zone also contains unique variations in sediment composition and compaction from site to site. A detailed description of each site is in Appendix B. The following descriptions explain the stratigraphy from the surface down.

Surface Soil

The uppermost zone is the surface soil. The soil is highly vegetated with roots throughout the entire thickness, often extending to the next zone at each site. The minimum soil depth is 15 cm at site 1-1. The maximum soil depth is 25 cm at site 2-1. The presence of gravels in the soil zone increases both in size and density upstream from 1-1 to 3-1. The NFTR soil zone is dense, approximately 50%, with gravels up to 7 cm.

Silt Zone

The second zone down from the surface in most of the stream bank sections has a silt-dominated matrix. The silt zone begins beneath the soil zone, except at the NFTR bank where there is a 16 cm layer of sand and gravel beginning at 20 cm depth. The silt zone is generally a medium to light brown. Areas near the bottom of the zone at each site

become gray and red as the amount of clay increases. Sediment composition varies from site to site. Site 1-1 is mixed with fine-grained sand. Site 2-1 contains medium sand and gravel. Site 3-1 contains gravels up to 7 cm. The thickness of this zone at the NFTR and site 1-1 are both greater than 0.6 m. The zone thins upstream from 1-1 and the density and size of the gravel increases from up to 3 cm at site 1-1 to up to 7 cm at site 3-1.

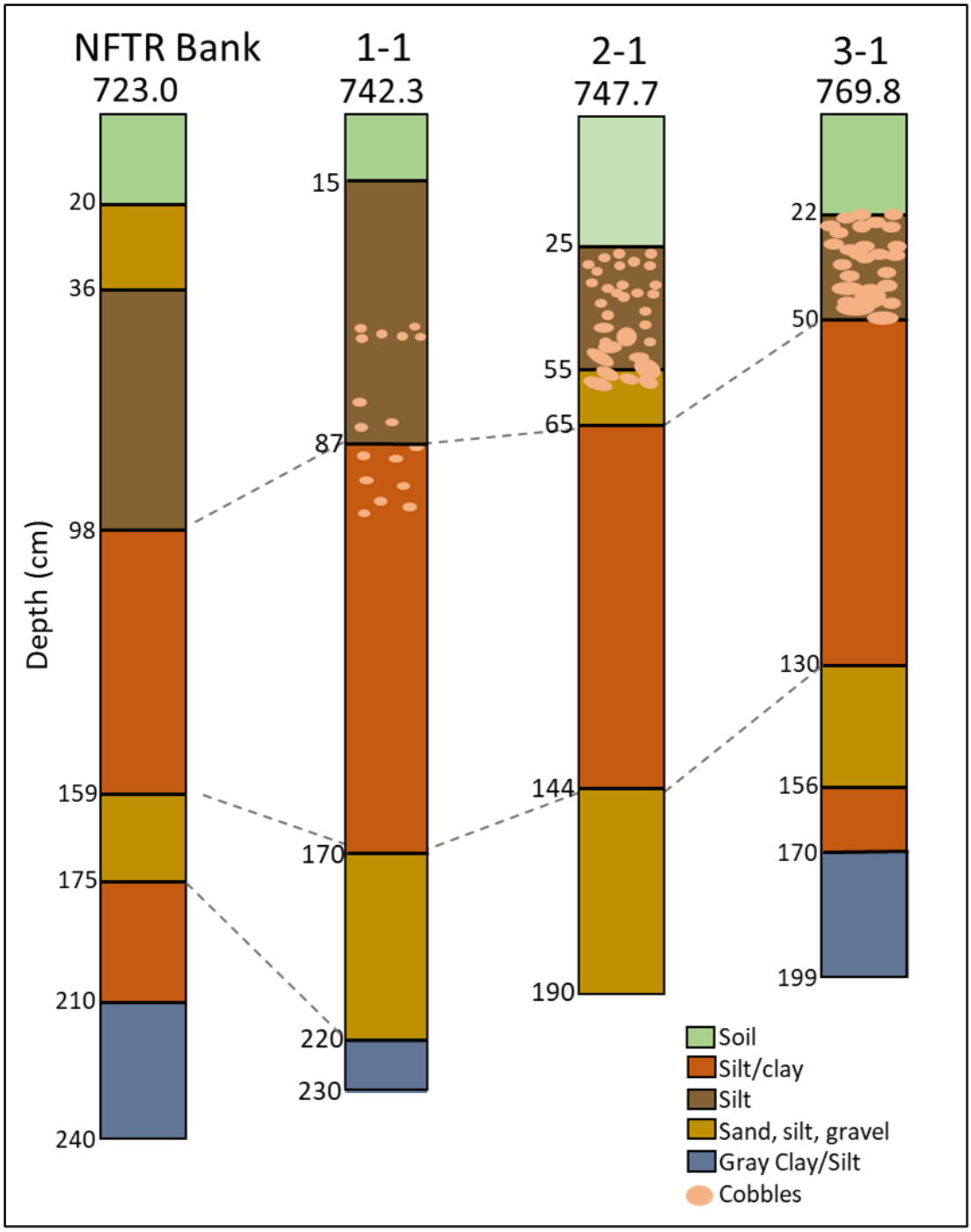

Figure 15. Streambank stratigraphy near the mouth of Indian Creek at the North Fork Teanaway River to 1.4 km upstream of Indian Creek. Locations are shown in Figure 5. Detailed descriptions of each site are in Appendix B.

Silt/Clay Zone

The third zone down is the thickest layer within the floodplain aquifer above the stream bed. The silt/clay zone at the NFTR bank is the thinnest described at 60 cm. The zone is thickest at site 1-1 at 83 cm. The concentration of clay increases with depth at all the stream bank sites. At some sites the clay concentration may exceed 70%. The lower portion of the zone is a predominant gray color at all sites. Evidence of oxidized rhizosphere are abundant throughout the zone. They are characterized by vertical streaks of brownish red clay in a gray clay matrix. Small lenses containing sand and pebbles are in this zone but vary by location. The upper and lower contacts contain sand and gravel.

Sand, Silt, and Gravel Zone

The fourth zone is composed of sand, silt, and gravel. The zone ranges from 15-cm thick at the NFTR bank up to greater than 50-cm thick at site 2-1. Gravel sizes at the NFTR and site 1-1 are not larger than 1.5 cm. Sites 2-1 and 3-1 each contain cobbles up to 10 cm. At sites 1-1 and 2-1 this zone extends to the stream bed and is the lowest exposed layer.

Gray Clay/Silt Zone

The fifth zone is a silty clay that is a bluish gray color. Site 1-1 silty clay contained no pebbles. Site 3-1 contains small pebbles at the top of the zone, but they are not present further down in the zone. This zone is not visibly exposed at sites 1-1, 2-1, and the NFTR. Excavation beneath the stream bed was required to reach it at sites 1-1, 3-1, and the NFTR. No excavation into the stream bed occurred at 2-1, so the zone was not seen there. The zone is about 30 cm thick at the NFTR and 3-1. It was only 10 cm thick

where it was observed at site 1-1. This zone at the NFTR site contains fine sand particles. At sites 1-1 and 3-1 it is sticky, plastic, saturated clay. Below this zone, not described in the stratigraphy, is sand, gravel, and cobbles; seen at the NFTR, 1-1, and 3-1.

Floodplain Stratigraphy

Much of the stratigraphy at the floodplain sites was similar to that of the stream bank sites (Figure 16). The stratigraphy described near MP-1 and MP-2 (Figure 5) is consistent with the descriptions of the stream banks. The floodplain, like the stream banks, has slight to major variations dependent on the location chosen to describe. Some of the floodplain sites varied considerably from the stream banks. Detailed descriptions of the floodplain stratigraphy are in Appendix B.

The stratigraphy encountered at site 3-2 is unlike the other sites. Cobbles up to 14 cm occur down to 80 cm. The sediment is sand, silt, and gravel to 60 cm depth. A layer of silt/clay that contains cobbles is then present to 84 cm. An abrupt transition to sand occurs around 84 cm depth, then another abrupt transition to wood. The auger bored through an approximately 40-cm diameter log down to 124 cm. The sediment then returns to sand and gravel.

Other sites that contain variations are MP-2 and 5-1. The silt zone was not encountered during the description at MP-2. At 5-1, located on the slope of a ditch (Figure 5) the upper most layer is the silt layer that is covered in grass at the surface. There is an abrupt transition to dense clay at 40 cm. The clay is brown and very plastic. It is present down to 130 cm where it then transitions to a mixture of sediment from clay to gravels.

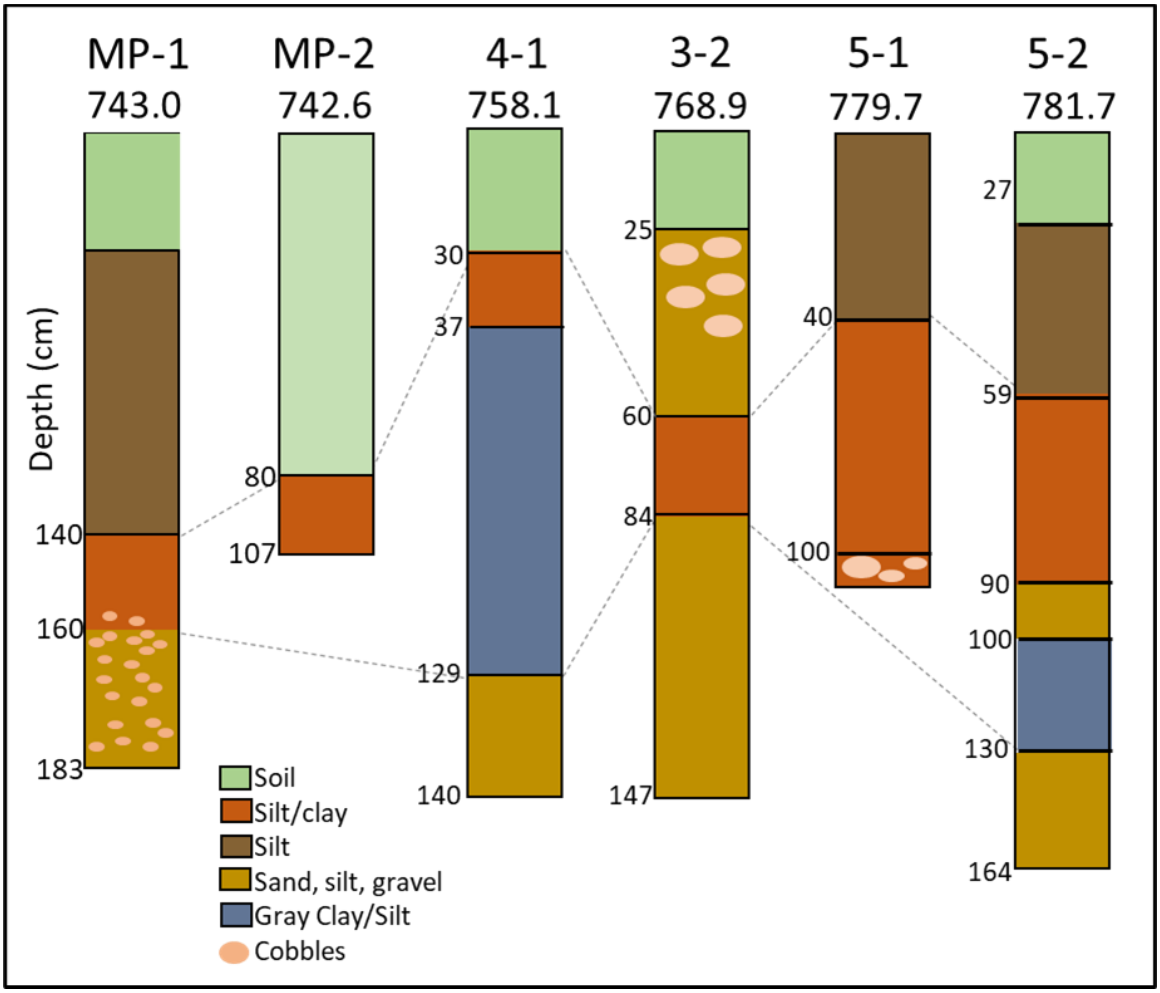

Figure 16. Floodplain stratigraphy. Locations can be seen in Figure 5. Detailed descriptions of the stratigraphy can be found in Appendix B.

Sediment Grain-Size Analysis

Grain-size analysis was conducted on nine samples. Samples 1-9 were collected from site 1-1. Sample 6 was collected from the middle of the range of sample 7, from 140 to 150 cm depth. All samples were sieved from 4 mm to 0.032 mm except the sample from unit 1. Unit 1 was not sieved through the 0.045 mm sieve due to an oversight. Some consolidated clay soil peds were unable to be crushed and separated by the pestle and mortar causing the mass to be added into a higher range.

The sieve results show the majority of the mass throughout the column to be 0.25 mm and smaller (Figure 17). Significant variation exists in the overall grain-size distribution of the column and within each zone. The silt zone shifts from a high percentage sediment <0.25 mm in the upper portion to a high percentage of sediment >0.25 mm in the lower portion. Results from units 5, 6, and 7 in the silt/clay zone show the zone containing a majority of sediment <0.25 mm.

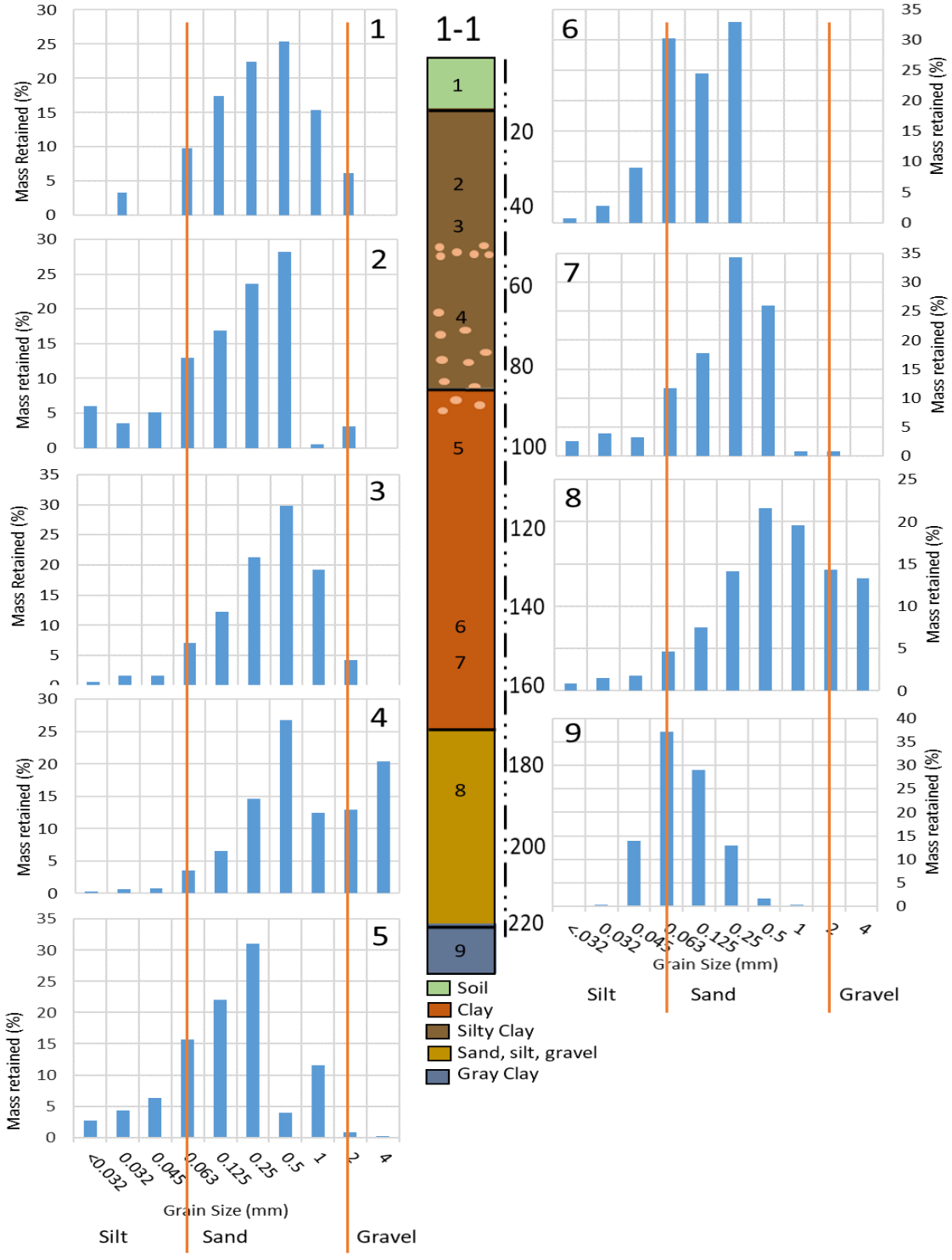

Figure 17. Sieve results from site 1-1 associated with the depth from which they were collected. Numbers in the upper left corner of the graphs correlate to the sample numbers on the stratigraphic column. Graphs show the grain size analysis as mass percent for each sieve range. Sieve sizes are in millimeters. Clay is <0.004 mm and contained within the <0.032 bin.

Samples 2-10 were also analyzed using the Mastersizer 3000 LV for the sediment-size distribution of the fine sediment within each unit sample. Mastersizer results show the size distribution of all unit samples after the removal of all grains larger than 0.5 mm. Results from the units from the silt/clay zone and the gray clay zone show the volume density percent of the units to be (Figure 18). The sediments within units 5, 6, 7, and 9 contain a large volume of grain-sizes of silt and smaller. Masses of the samples and graphs from each unit are in Appendix C. These results confirm the results of the sieve data and show the volume of fine sediment within the zones.

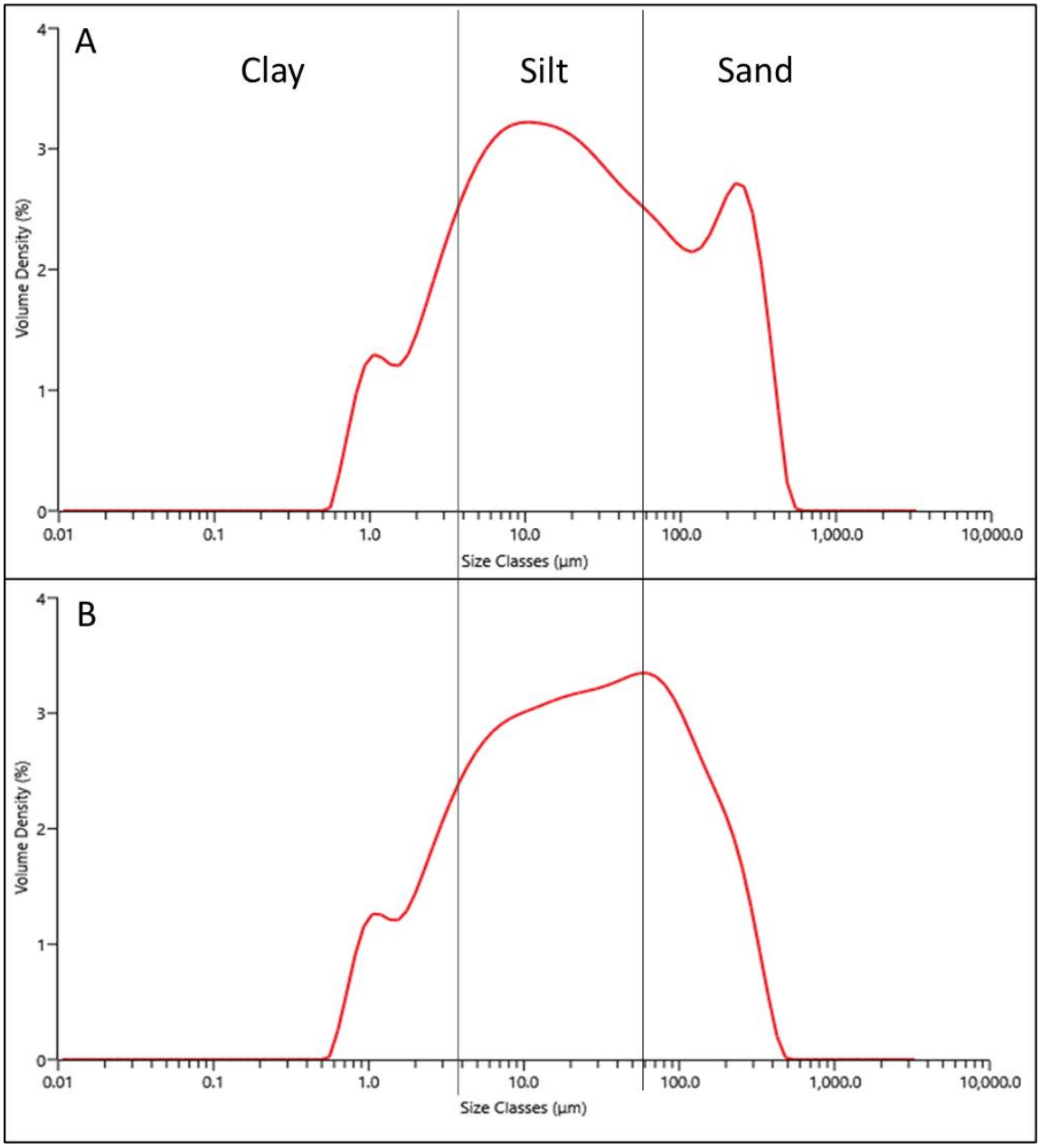

Figure 18. Mastersizer results. Graphed results shown are from the zones within stratigraphy site 1-1 that contain the most clay and least amount of sand and larger sediments. A) represents unit 5, B) represents unit 6, C) represents unit 7, and D) represents unit 9. Mastersizer graphs of the remaining units are in Appendix C.

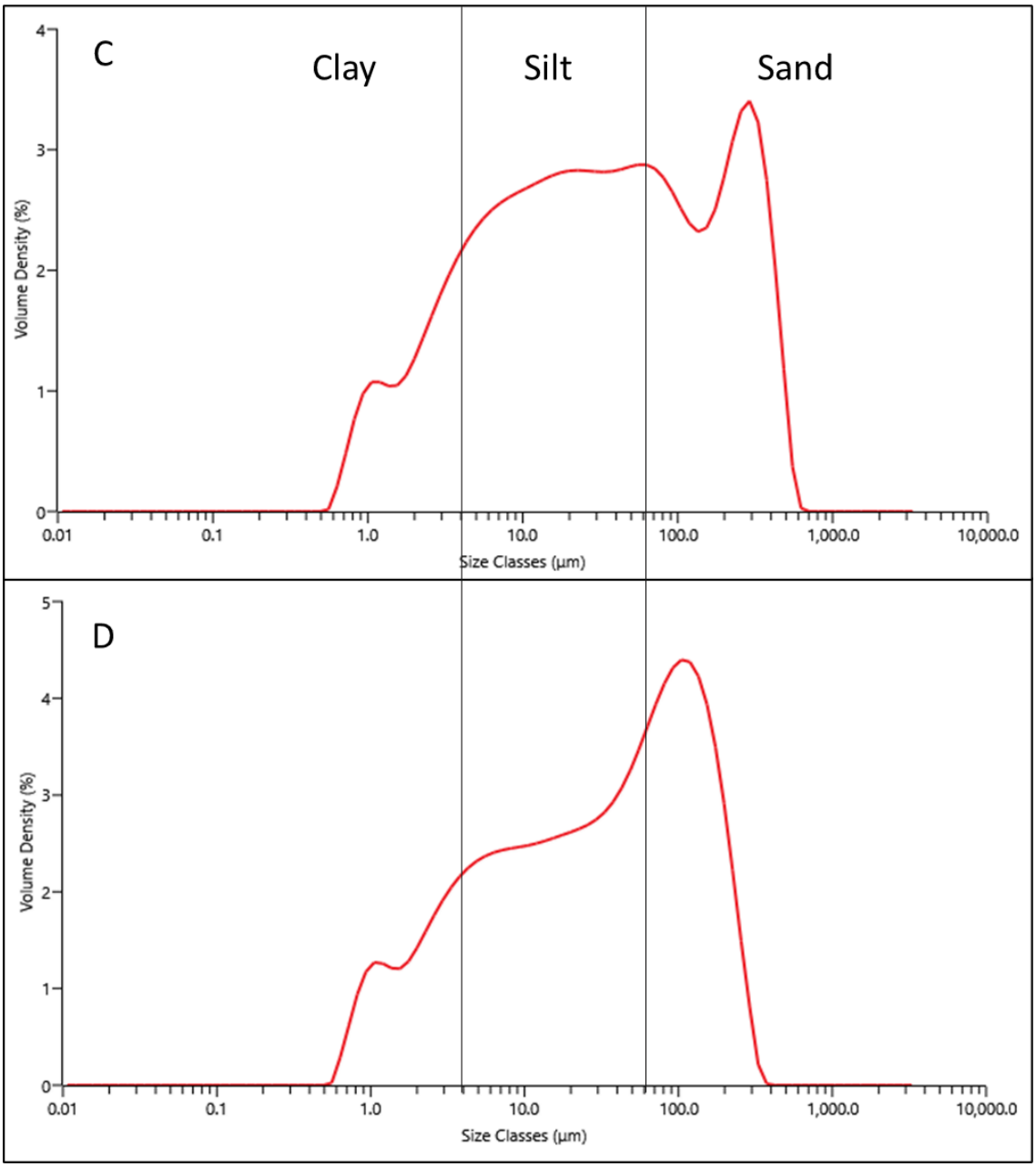

Figure 18. Mastersizer results. Graphed results shown are from the zones within stratigraphy site 1-1 that contain the most clay and least amount of sand and larger sediments. A) represents unit 5, B) represents unit 6, C) represents unit 7, and D) represents unit 9. Mastersizer graphs of the remaining units are in Appendix C.

Porosity

Porosity estimates were calculated to gain an understanding of the storage potential of the aquifer (Figure 19). The estimates are also useful for calculating the permeability of the different stratigraphic zones within this area of the aquifer. Estimated porosity values for units 1-4, 7 and 8 were calculated using HydrogeosieveXL. Average porosity for these units is approximately 0.33. Porosity values for samples 5, 6 and 9 are based on estimations from Schwartz and Zhang (2003). Similarities in the higher porosity values for samples 5,6, and 9 are related to those units containing approximately 15% sediment smaller than 0.045 mm (Figure 17).

The porosity estimates for this stratigraphic column do not necessarily reflect the entire floodplain. These samples were taken from the stream bank at section 1-1 and therefore are only useful for interpreting porosity for this area. The stratigraphy of the floodplain and composition of the zones vary throughout the entire reach (Figures 15 & 16).

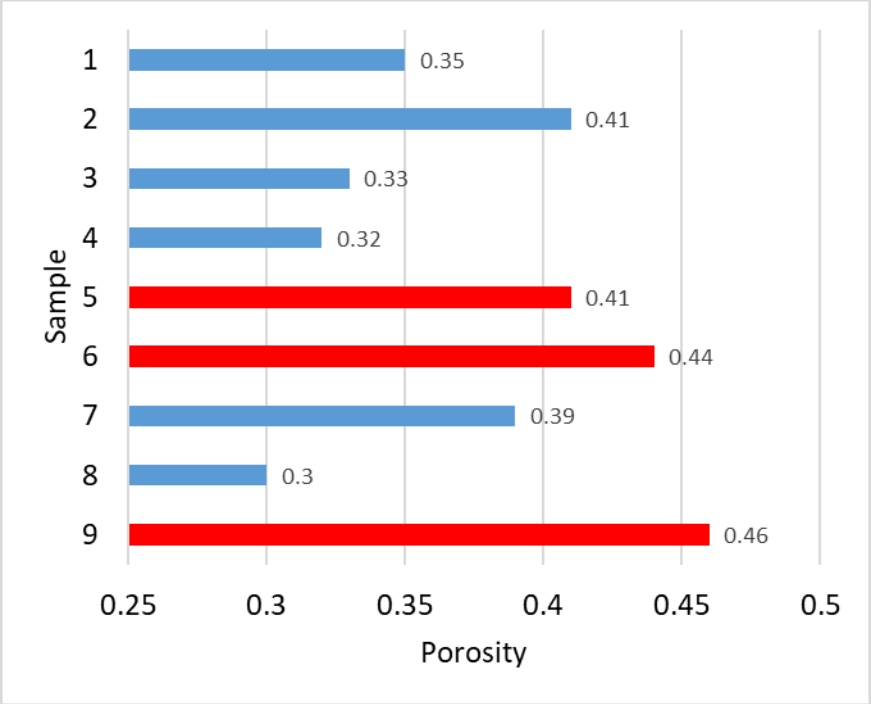

Figure 19. Porosity for site 1-1. Values in blue were calculated using HydrogeosieveXL. Values in red were calculated using values from Schwartz and Zang (2003).

Streamflow Model

HEC-RAS hydraulic flow model of the Indian Creek comparisons were performed to gain an understanding of the change in water-surface elevation (WSE) with instream LW. The purpose was to determine how high up the 2-meter-tall stream banks the WSE is likely to rise with and without LW under average and peak spring discharges on Indian Creek. This would help determine if the addition of LW increases the WSE to levels where it intersects the more permeable layers of the floodplain stratigraphy for a greater vertical distance or for a longer period of time, or whether it overtops the banks.

The model results show the addition of LW in the stream channel causes an increase to the WSE (Figure 20). Differences in WSE between the two modeled scenarios increase with increased discharge (Figure 20). Mapped results from the model show floodplain inundation increase with increased discharge (Figure 21). The areas of inundation are areas the LiDAR determines as the same elevation as the stream, which causes the model to place water in the area. The increase is not necessarily due to overbank flow. Cross-sectional views show that at the highest flow the water is unable to overtop the banks (Figure 22). Detailed outputs from the model are in Appendix D.

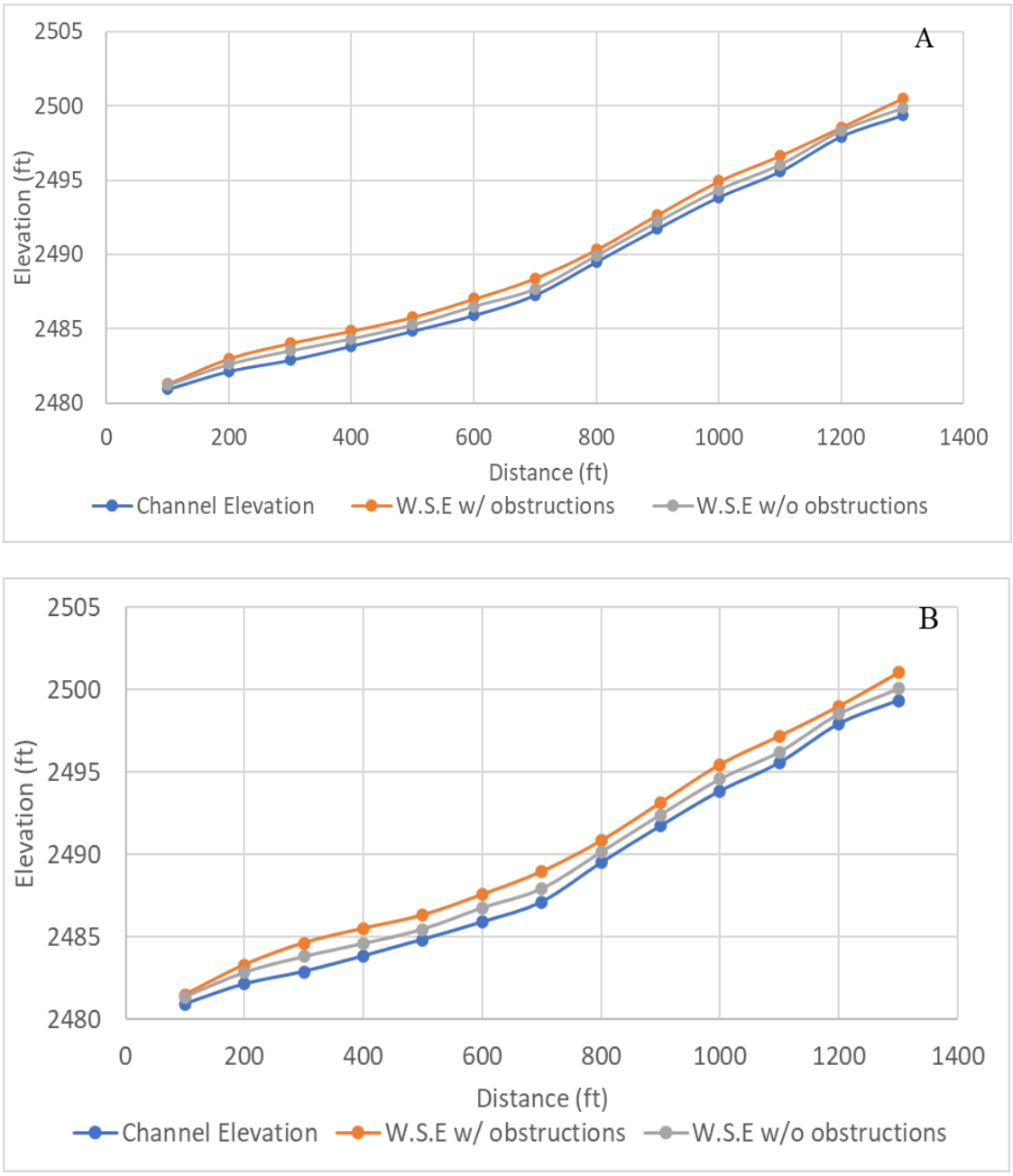

Figure 20. HEC-RAS model results. Water surface elevation comparison of the four modeled discharges. A) 6.0 ft^3/s, B) 13.4 ft^3/s, C) 15.9 ft^3/s, D) 36.4 ft^3/s. The gray line represents the WSE without obstructions. The orange line represents the WSE with obstructions. The blue line represents the minimum channel elevation. Detailed outputs from the model are in Appendix D.

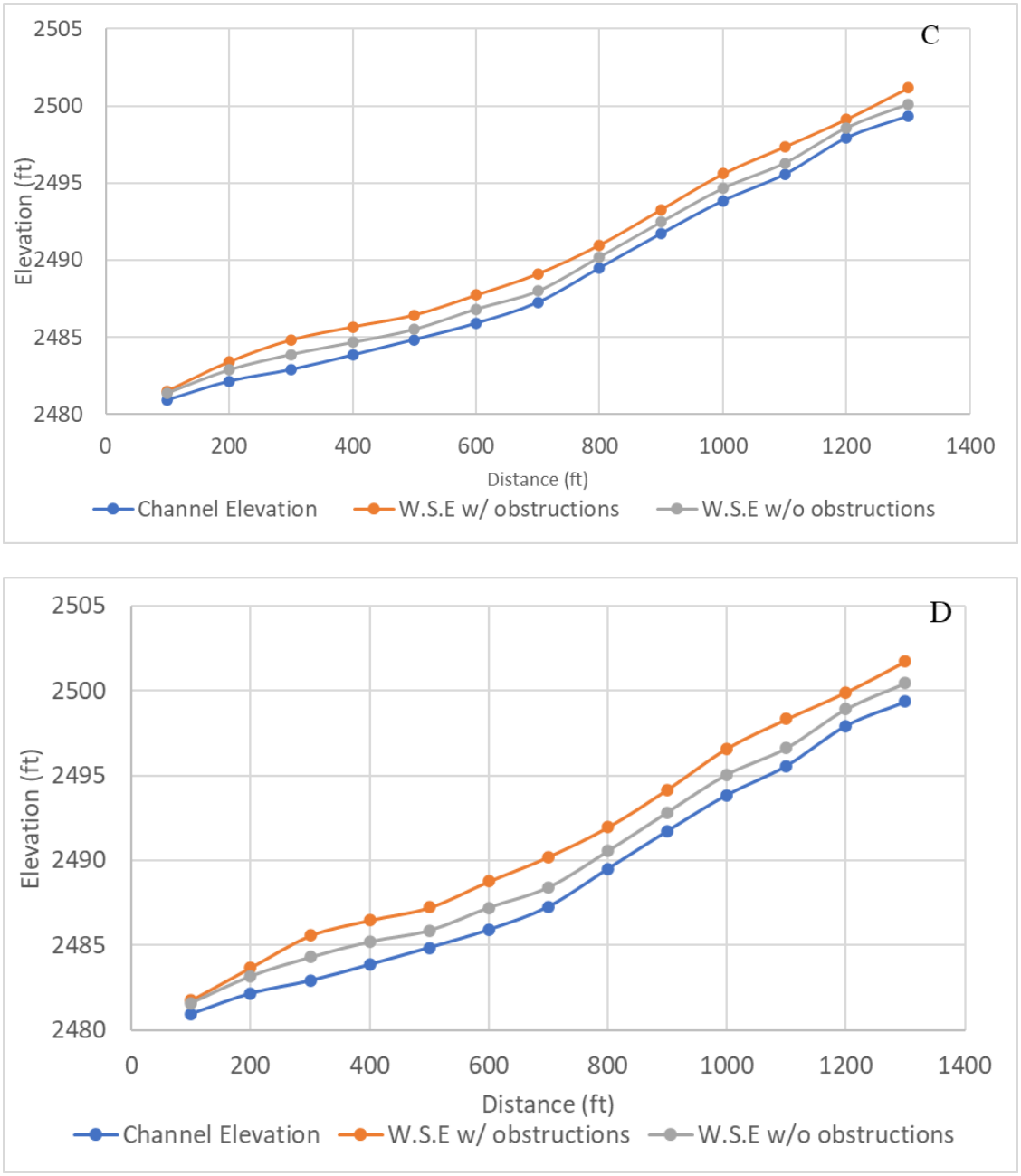

Figure 20. HEC-RAS model results. Water surface elevation comparison of the four modeled discharges. A) 6.0 ft^3/s, B) 13.4 ft^3/s, C) 15.9 ft^3/s, D) 36.4 ft^3/s. The gray line represents the WSE without obstructions. The orange line represents the WSE with obstructions. The blue line represents the minimum channel elevation. Detailed outputs from the model are in Appendix D.

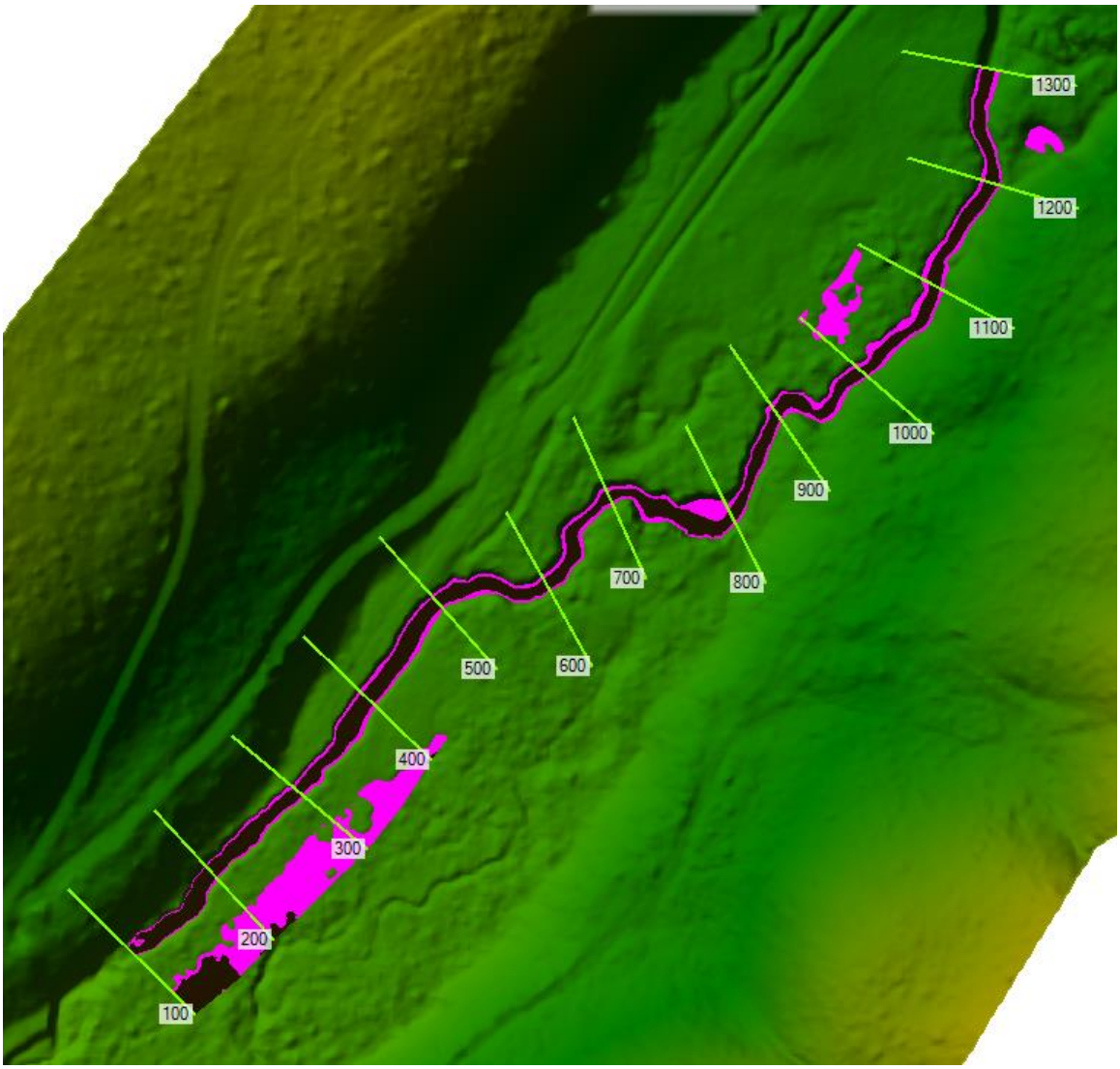

Figure 21. Map of the stream stage model results. Results of the 36.4 ft^3/s discharge models. The dark color represents the water surface elevation without obstructions. The bright pink color represents the water surface elevation with obstructions.

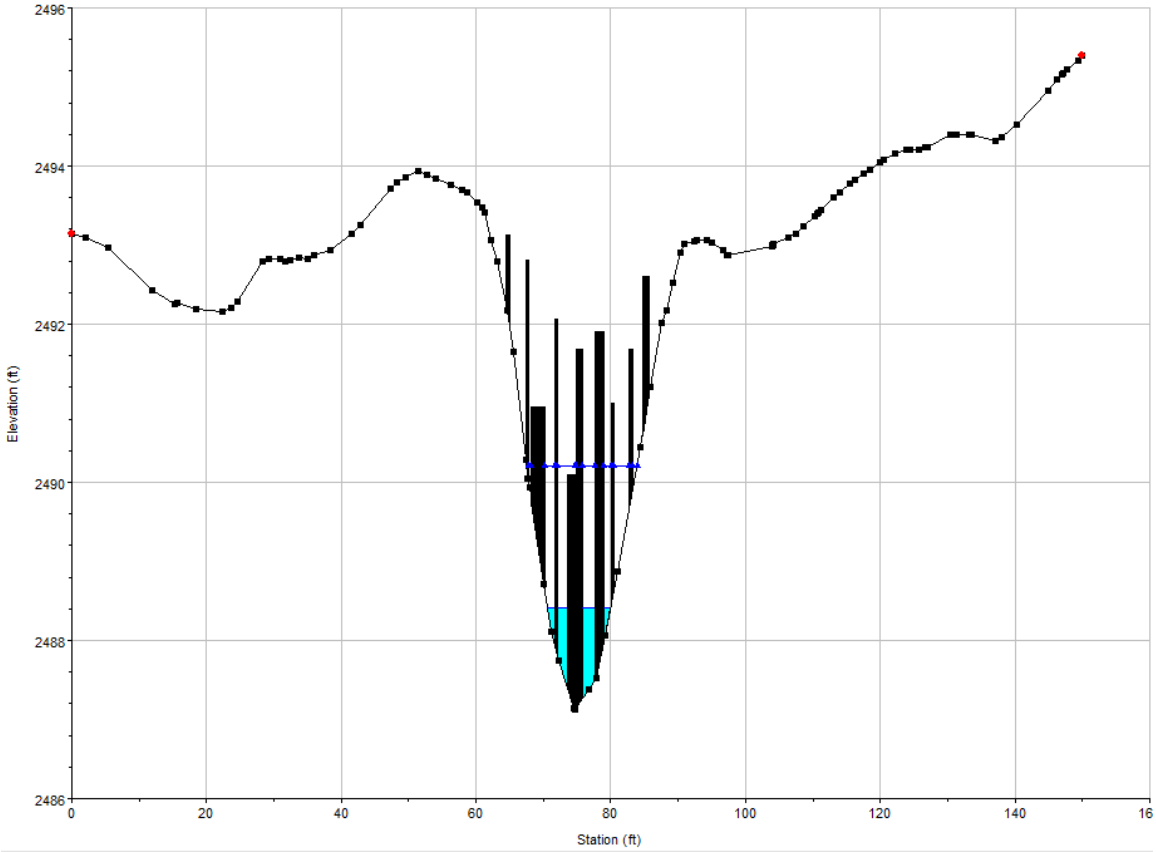

Figure 22. Example cross-section with instream obstructions of the difference in water surface elevation (WSE) with and without obstructions in the channel of the 36.4 ft^3/s model. This is the cross-section located at 700 feet up the reach. The blue line with triangles represents the WSE with instream obstructions. The light blue filled area represents the WSE without instream obstructions.

CHAPTER IV

DISCUSSION

Groundwater

If the wood in the stream channel is influencing GW recharge and storage in the floodplain, the data should show an overall increase in GW levels and/or duration before returning to summer low levels. Increases to the peak levels would be seen in the early spring or late winter during the snow melt. A sustained duration of the increased GW would be seen in the late spring or early summer.

The differences and similarities between the two well clusters allowed a comparison of the spatial and temporal variations in GW levels, which contributed to the interpretation of the possible effects of instream LW. The two clusters are separated by about 1.5 km (Figure 5) distance and around 40 m in elevation (Table 2). The downstream cluster is located approximately 0.1 km upstream of the most densely placed instream wood of the LW restoration project (Figure 4 & 5B). There has been no instream LW emplaced within 0.5 km of the upstream cluster. This difference in proximity to the instream LW implies that the downstream cluster is more likely to experience changes to GW recharge or storage from the wood restoration.

The long-term GW activity is best interpreted in the data of wells MP-1 and MP-4 because these wells contain the longest and most continuous record since monitoring began in 2014 (Figures 10 & 11, Table 4). Comparison of the other wells requires separate interpretations of the pressure transducer data and the manual measurements. Manual measurements aided in clarifying some of the pressure transducer data (Figures

12, 13 & 14). The precise elevations of the manual measurements correct many obscure data recorded by the pressure transducers and the illustrate the differences in rates of change of the water levels in the wells (Figure 14).

Downstream Wells

Because MP-1 and MP-5 are closer to the stream than MP-2, it would be expected that they would show an increase in GW levels before MP-2 during times of recharge if the stream water is a significant source of input from the stream banks (Figure 12). MP-1 goes dry every year, thus there is a delay in the presence of water in the well when the GW is being recharged. The groundwater in MP-5 increases at the same time as MP-2, but not at the same rate (Figure 12). Since MP-5 was recorded as dry on 08/26/2020, there was likely a delay in the presence of GW in the well, producing an increase in GW of approximately 1 cm at the next reading on 10/21/2020. Because both MP-1 and MP-5 have delays in the presence of GW, the wells do not provide adequate information to determine if the GW in MP-1 or MP-5 begins to increase before MP-2.

MP-1 and MP-5 are two of the shallowest wells of the two clusters. MP-1 is located at a highpoint of the floodplain. This depth and location of MP-1 are the reasons the well goes dry each year (Figure 23). MP-5 reaches nearly the same depth as MP-1 but is located in the middle of the floodplain at a low point 2.2 meters lower than MP-1. MP-5 has been recorded as dry once and nearly dry on five occasions (Figure 12). It is not possible to know the water level in the area of these wells when they are dry. Manual measurements suggest that if MP-5 is dry, the water level is not far beneath the depth of the well. MP-1 is dry for a longer period each summer than MP-5, suggesting that the

water level drops further beneath the bottom of the well (Figure 12). The water level in MP-2 could be an indicator of the water level beneath MP-1 during the dry months (Figure 23). Using the GW level of MP-2 suggests the water may be present approximately 0.5 m beneath MP-1 on 6/28/2020.

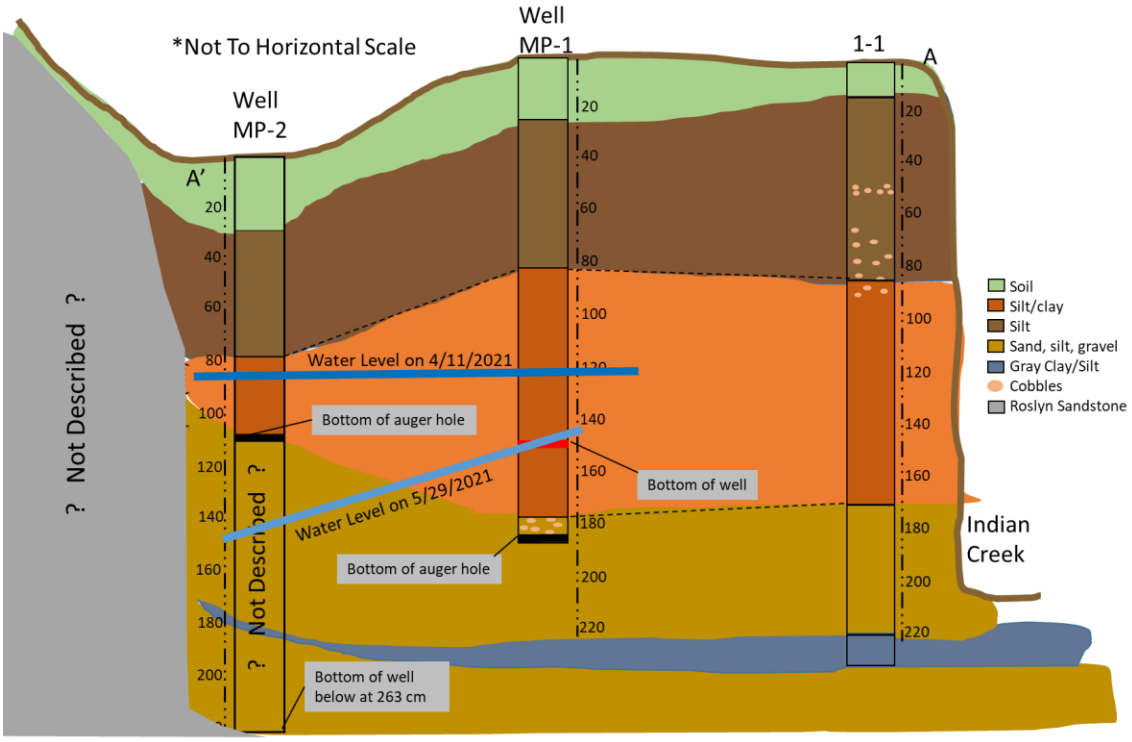

Figure 23. Cross-sectional interpretation of the stratigraphy of the floodplain at the downstream wells from the hillside to the streambank. The Stratigraphy of site 1-1 was placed as the stream bank stratigraphy due to the similarities in stream bank stratigraphy. Water lines show the depth of the water in MP-1 and 2 on 4/11/2021 and 5/29/2021. The dates of the groundwater levels shown here are the same dates in groundwater gradient figure (Figure 24)

Pressure transducer data from MP-2 shows the possible increase in summer base level GW level since monitoring began until the device malfunctioned in 2017 (Figure 11). The increase was noted by Boylan (2019) with the possibility that the increase is attributed to the LW installation. It is more likely that the increase to the base level GW is attributed to particularly high precipitation from May-August 2016 (Figures 10 & 11). Later manual measurements from MP-2 show that the increase in the minimum GW elevations during the summers from 2014-2017 did not persist through the subsequent years. The manual measurements show the summer base level returning to an elevation similar to when the transducer was installed in 2014. Precipitation during the summer months from 2017-2021 returned to low-moderate levels.

Comparisons of precipitation, GW elevations, and stream discharge illustrate the interactions between the surface water and GW before and after the LW emplacement (Figure 10). Increased and sustained GW levels at all the wells in the downstream cluster are often associated with monthly precipitation levels above 70 mm during the months when precipitation is likely to fall as rain. The annual springtime peaks in the GW levels and stream gauge data consistently occur after the peak in winter/spring precipitation. However, the peak discharge in the stream tends to occur after the peaks in GW levels in the wells, in some cases when MP-1 is already nearly dry. This indicates that the peak stream flow is not a significant source of recharge to the floodplain GW.

Upstream Wells

The upstream wells provide a basis for comparison with the downstream wells because their distance from the restoration makes it improbable that the GW levels are directly affected by the instream LW. MP-4 is located on the north side of the floodplain near the hill. A two-meter ditch that runs parallel to Indian Creek is approximately 10 meters to the north, between MP-4 and the hillslope (Figure 5). Nearly identical timing in the water-level fluctuations occur in MP-4 in the upstream cluster and MP-1 in the downstream cluster. This similarity indicates that the GW throughout the reach is responding uniformly to the same factors affecting the inflow and outflow of water from the floodplain aquifer.

The water in the upstream wells behaves somewhat differently at times than would be expected. This is evident in the manual measurements taken in October 2018 and those taken from August and October 2020 (Figure 13). In October 2018, the water level in MP-4 increased faster than the water level in MP-3. However, in 2020 the water of MP-3 increased at a faster rate than MP-4. Because these wells are unlikely to be affected by the wood restoration, it appears that other factors are responsible. This may be due to a difference in the stratigraphy between the two well locations causing differences in the timing and sources of GW flow into and out of the wells.

In contrast to the downstream wells, none of the upstream wells have been recorded as dry since monitoring began. MP-4 and MP-6 are the deepest wells in the cluster, both usually contain at least 0.5 meter of water above the bottom of the well (Figure 11). MP-3 is the shallowest well of the two clusters at less than a meter depth.

The stratigraphy near MP-3 shows that the bottom of the well is in the sand and gravel zone above the gray clay (Figure 16). When manual water measurements were taken in both MP-3 and MP-6 during the summer and autumn the water has smelled like sewage. The foul-smelling water could mean that once the spring peak water levels have subsided there is a stagnant perched water table on top of the gray clay layer at these two wells, but not at MP-4. The difference at MP-4 is likely that the depth of the well penetrates through the gray clay into the sand and cobbles observed at site 3-1 and the NFTR streambank.

Again, the missing data of the wells and the stream discharge make a full comparison of GW elevations, precipitation, and stream discharge difficult. The GW elevations of the upstream wells show similar patterns to the downstream wells when compared to the precipitation and stream discharge (Figure 11). The pattern shows the GW elevations increasing following the major winter/spring precipitation and melt. The peak stream discharge often occurs after the GW levels have started to decline. In 2021, peak GW level was not recorded by the pressure transducers. The manual measurements from 4/11/2021 are in line with peak discharge for 2021 in both upstream and downstream wells. This may have been the time of peak GW and peak discharge due to the high volume of snow that fell in late winter.

Pressure Transducer Data

The rapid fluctuations of the GW levels shown by the pressure transducer data may be due to warm and cold weather periods. Without exact temperature data or information on how much precipitation fell as snow or rain each year it difficult to understand the source of the rapid fluctuations in each year. If the rapid GW fluctuations

are due to changes to atmospheric temperature, this would suggest that the water is flowing through a highly permeable zone confined beneath a zone of much lower permeability. When a period of daytime temperatures produce snowmelt the GW level in the well increases rapidly. If the daytime temperature does not produce much melting, the GW level may decrease rapidly. If temperatures are cold and melt does not occur, water levels may rapidly decrease from the piezometer as the water level decreases in the sand and gravel zone. When temperatures warm and melt begins, water can quickly saturate the thickness of the sand and gravel zone, pushing water up the piezometer.

Some of the fluctuations are likely inaccurate pressure measurements from the pressure transducers. At times the measurements change by more than 0.5 m within a single day. This rapid movement of water within the ground is unlikely to occur during the wet part of the water year and has not been recorded with any of the manual measurements (Figures 10 & 12). However, none of the manual measurements have been taken from the months of November through March, which is when the most rapid fluctuations tend to occur.

Groundwater Summary

MP-1 and MP-4 pressure transducer data do not indicate an increase to the duration of high GW levels above the summer low level since the wood emplacement began in 2015. The duration that GW remains above the summer low levels varies from year to year (Figures 11 & 12) (Table 4). The date that MP-1 goes dry each year ranges from early April to late May. The duration that monthly precipitation remains above 70 mm is directly correlated to the duration GW levels are sustained at MP-1. MP-4 GW

levels react with each period of precipitation above 70 mm per month (Figure 11).

The peaks in groundwater levels are typically preceded by a peak in monthly precipitation. This pattern was observed in the data from all of the wells, as shown in Figures 10 & 11. Specifically, in November 2015 monthly precipitation reached 247 mm, the following month reached 322 mm. This period of above-average precipitation led to a large spike in the GW elevation at all of the wells that were in place at that time (Wells 1-4). Although precipitation remained high, above 75 mm per month through March, the water table of MP-4 declined rapidly at the end of December. It is likely that most of the precipitation that fell in January and February fell as snow and did not infiltrate into the subsurface until the melt in March. There is, however, a spike in January that may indicate that some of the precipitation fell as rain. The pressure transducer at MP-1 for this time shows many rapid fluctuations in water level and it is difficult to discern whether or not these are actual levels or erroneous readings.

The data from the wells and stream gauge at Indian Creek indicate that the stream water during peak discharge is not a primary source of GW recharge to the floodplain. If the stream were a predominant source of recharge to the GW, the peak annual discharge should occur prior to the annual peak in GW levels. Peak discharge of the stream usually occurs after the GW levels have peaked and begun to decline (Figure 10 & 11). An exception occurred in 2019 when stream discharge peaked on 04/07/2019 and the GW level in MP-1 peaked on 04/10/2019. The peak GW level on 4/10/2019 followed a four period of monthly precipitation exceeding 100 mm beginning in December and ending in March. This pattern of the peak stream discharge lagging the highest groundwater levels

is observed both before and after the period when the wood was installed in the channel.

Manual measurements from the wells can be used to determine the general direction of the GW gradient (Table 3). GW elevations in the wells of the downstream well cluster suggest the GW gradient at the cluster slopes down valley during the recharge and peak GW elevations (Figure 24A). As GW elevations in the wells decline the GW gradient may slightly increase away from the stream. The water within the wells at MP-2 and MP-5 decline as a faster rate than the water in MP-1. Similar patterns are seen at the upstream wells (Figure 24B). The GW in the pipes of MP-3 and MP-4 are near 10 cm different, sloping towards MP-4. At the end of May, there is a 1.2-m difference between the GW elevations in the pipes. This suggests GW gradient may be increasing to the north as the water drains from the floodplain aquifer. The rate of decline in GW present in MP-6 is similar to the rate seen in MP-3. The rates of decline of the GW in the wells may not be completely related to the GW gradient but may be more closely related to how the stratigraphy of the floodplain aquifer affects the rates of decline in the varying depths of the wells.

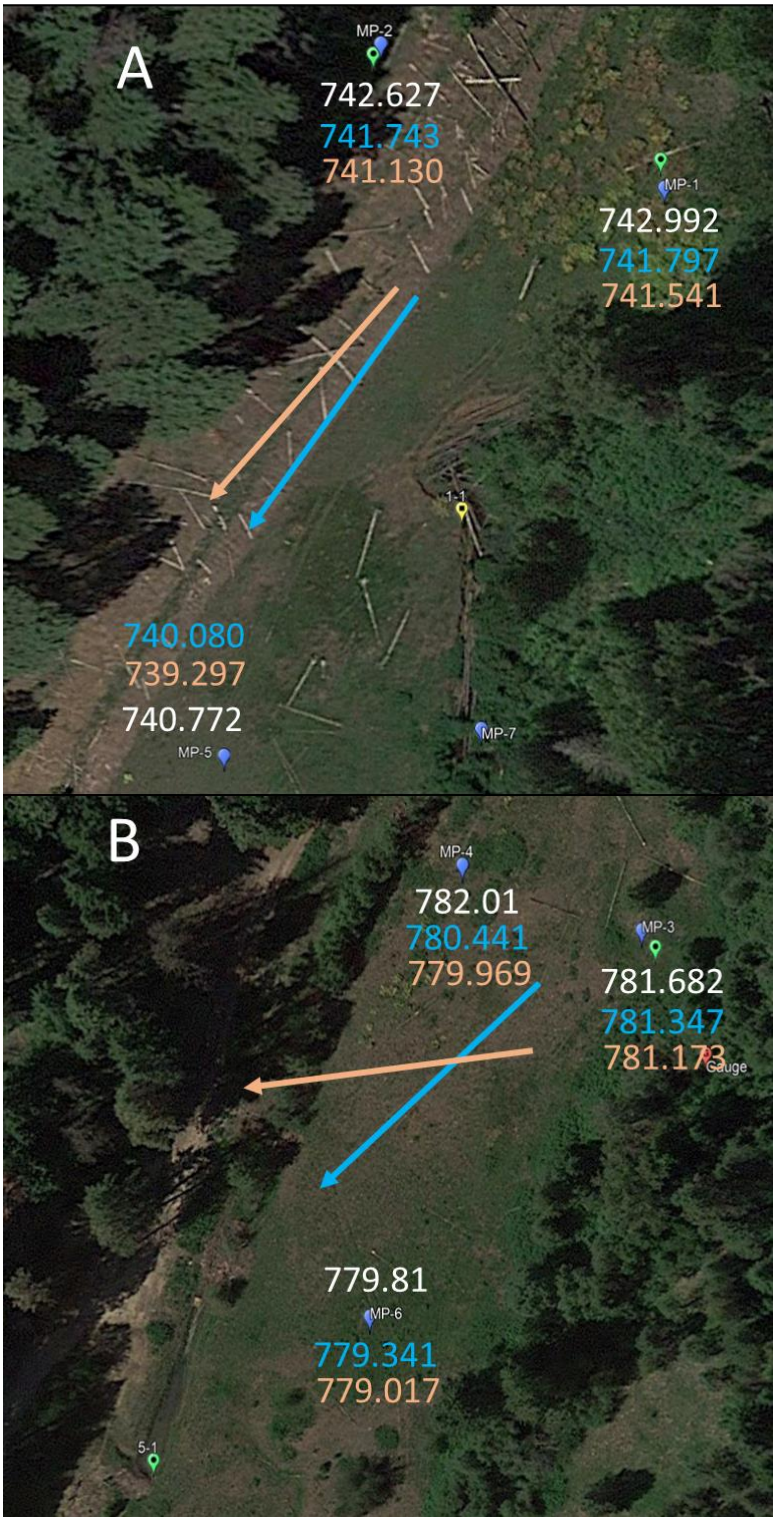

Figure 24. Changes in groundwater levels from spring 2021. Image A shows the downstream wells. Image B shows the upstream wells. White numbers are surface elevations. Blue numbers are groundwater levels taken on 4/11/2021. Orange numbers are groundwater levels taken on 5/29/2021. Colored arrows correlate to the colored numbers and represent the groundwater gradient estimates.

Stratigraphy and Floodplain Aquifer Characteristics

The stratigraphy at Indian Creek could affect the recharge, storage, and movement of GW throughout the reach. The differences in sediment throughout the depth of the described areas of the reach may have differences in permeability that could retard the flow of water through the banks and down from the surface. If the aquifer were to be recharged from bank infiltration, it would most likely occur through the sand and gravel layer above and below the gray clay. The gray clay may be acting as a semi-confining layer throughout much of the floodplain, causing water to be perched in the sand and gravel above it, or at least not move downward as readily as it could through the more permeable layers of coarser sediment.

The differences in sediment composition can account for considerable differences to aquifer properties such as porosity, permeability, and hydraulic conductivity depending on other factors such as compaction and saturation (Richard et al., 2001). The sediment analyzed for grain size was collected from the stream bank at site 1-1 and is not necessarily representative of the ratios of silt and clay in similar zones throughout the floodplain. It was clear in the field that the clay content of the silt/clay zone found at sites 5-1 and MP-3 was predominantly clay. The estimated porosity of the silt/clay zone and the gray clay is considerably higher than the other zones in the aquifer. Because the permeability and hydraulic conductivity of silt and clay is several orders of magnitude less than sand and gravel, it is likely the silt/clay and gray clay zones impede the flow of water throughout much of the thickness of the floodplain aquifer.

The rapid change in water level in the wells suggests the water is readily moving

through a highly permeable zone (Figure 10 & 11). Most of the wells penetrate into or deeper than the sand and gravel layer above the gray clay. MP-4 and MP-2 very likely extend through the gray clay while MP-3, 5 and 6 end in the sand and gravel. Stratigraphy from approximately three meters north of MP-1 shows that the bottom of the well reaches 30 cm from the bottom of the silt/clay zone. If the bottom of MP-1 is located within the silt/clay zone, then the permeability of this zone must be nearly the same as the permeability of the sand and gravel zone. Irrespective of possible differences in permeability of the stratigraphic zones throughout the reach, the GW levels in the wells change rapidly.

The gray clay layer is the stream bed in many areas of the stream, including near site 1-1. The clay was not penetrated by the auger at the floodplain stratigraphy sites, except for in the ditch near MP-4, because the sand and gravel layer prevented further excavation. Because the clay was found in the ditch near MP-4, it is likely it would be found further downstream on the same side of the floodplain at MP-2. The gray clay began at 2.20 m at site 1-1 and was approximately 20 cm thick. The bottom of MP-2 reaches 2.63 m depth, likely deeper than the gray clay layer (Figure 23). Because MP-2 has not been recorded as dry, it is possible that water either sits perched on top of the gray clay or the well is penetrating into deeper portions of the floodplain aquifer than the surrounding wells in the downstream cluster.

Many areas of the channel are shallow with banks not exceeding 20 cm or are gradually graded to the ground surface. These areas experience annual overbank flow during the high discharge season, with and without instream wood, which causes large

amounts of water to flow across the surface of the floodplain after the snow has melted. The areas of shallow banks are not in reaches where dense LW was installed and thus floodplain inundation is likely due to other factors.

Precipitation and snowmelt are the dominant contributors of GW recharge. It is unclear whether the water that recharges the GW comes directly from the surrounding hills and higher elevations or if much of it comes from the floodplain surface meltwater. If the floodplain surface meltwater contributes to the GW recharge it must percolate downward nearly 2 meters through the silt and clay dominated sediments. On 04/17/2020, at the time of peak stream flow, the ground surface was noted as "very dry" although some snow was still present in small amounts. This is also the date that MP-1 was recorded as dry for the first time that year (Table 4).

Discussion of Potential Storage Capacity

The porosity values were calculated to assess the potential storage capacity of the aquifer. Due to the vertical heterogeneity of the floodplain stratigraphy throughout the reach, an estimation of potential GW storage based on porosity values from one site would yield highly inaccurate values (Huggenberger and Aigner, 1999). The porosity values for site 1-1 show the units within the zones containing high clay content are much more porous than the surrounding zones (Figure 18). The thicknesses of the stratigraphic zones, although remarkably similar at the streambanks, show significant variation throughout the floodplain (Figures 15 & 16). In many areas, the clay content is significantly more, which may increase porosity but reduce permeability, thereby reducing GW recharge and storage potential.

The potential storage capacity was calculated for maximum and minimum estimations (Table 5). The area used is from the furthest downstream well, MP-6, and the furthest upstream wells, MP-3 and 4. The area was estimated by drawing a polygon on Google Earth Pro and was rounded to 126,000 m^3 (Figure 25). The depth to bedrock values were estimated by using an average depth from the top of the ubiquitous sand and gravel zone down to possible depths to bedrock of 3.5 and 6.5 meters. A third calculation was performed to estimate the potential storage of the floodplain aquifer above the sand and gravel layer. For the minimum and maximum storage potential calculations of the depth to sandstone bedrock, estimated values of 0.69 and 0.81 permeability, and 0.1 and 0.3 specific yield (Johnson, 1967). The zones above the sand and gravel zone are not included in the calculations for depth to sandstone bedrock because of the abundance of fine sediment with low specific yield. A permeability of 0.4 was used for the calculation of storage potential for the sediment above the gray clay. The same values for specific yield used in the first two calculations were used in the calculation of sediment above the gray clay.

Table 5. Potential Storage Capacity. Calculated estimates of the potential storage capacity of the Indian Creek floodplain aquifer for the area shown in Figure 25 (126,000 m^2). Depths to bedrock are estimated from an average value of the top of the sand and gravel zone beneath the silt/clay zone.

Depth to Bedrock	Min. Volume (m)	Min. Volume (ac-ft)	Max Volume (m)	Max Volume (ac-ft)
2	10080	8	30240	25
3.5	30429	25	91287	74
6.5	66339	54	199017	161

Figure 25. Area polygon used for potential storage capacity. The polygon extends from the furthest upstream well to the furthest downstream well; from the approximate location of the stream channel to the northern hillside.

Recent floodplain restoration work in the fall of 2020 near the upstream well cluster filled an approximate 2-meter incised drainage channel with large piles of small woody debris (SWD) and dirt. The SWD piles are spaced so that pools of water develop between them. At the end of winter, the spaces between the SWD contained enough water to fill the depth of the channel. Water remained in most of the pools throughout the summer of 2021, creating stagnant ponds. The gray clay/silt zone was found just beneath the bottom of the channel prior to the SWD installation. A ponded portion of the channel is located approximately 10 meters northwest of MP-4 (Figure 5). The presence of the pooled water so close to the well did not have a noticeable effect on maintaining or increasing the GW level in MP-4 or MP-5 (Figure 12). The lack of change to the GW levels in the wells might be related to the GW flow direction results noted by Boylan (2019) showing the GW at the upstream wells flows northwest, away from Indian Creek (Figures 23 & 24).

Streamflow Model

By placing large wood piles in the channel of the stream, the water is displaced, thereby increasing the flow stage for a given discharge. The instream obstructions increase the possibility of overbank flow during high flow periods (Wohl, 2013). Simulated channel obstructions were placed in the streamflow model at cross-sections located every 100 feet. The channel at Indian Creek contains continuous wood that densely fills the entire channel in much of the modeled reach. The model provides an example of how the WSE might change after the addition of wood.

Changes in stream stage before and after the channel wood restoration are not apparent in the Washington Department of Ecology stream gauge data. This may be due to several factors. Mainly, the stream gauge is located on the upstream side of a culvert and downstream of much of the large wood restoration. The culvert is large enough to allow for unimpeded flow on the downstream side. Instream large wood restoration has taken place downstream of the culvert but does not currently show any indication that it is increasing the back-up of water upstream of the culvert.

The streambanks at most areas of the modeled reach are approximately two meters tall. The channel depth becomes increasingly shallow downstream and is covered by thick vegetation where the modeled area ends. Throughout the modeled reach the channel contains near continuous instream large wood piles (Figure 4). The water remains within the channel at all known discharge volumes.

Given the present geometry of the channel at Indian Creek, the HEC-RAS model results indicate that the increased streamflow obstruction from the LW is unlikely to have

a significant effect on the GW recharge or floodplain inundation. The hydraulic simulations show that during the highest recorded discharge at Indian Creek of 36.4 ft3/s on 05/05/2017, the stage is unlikely to fill the channel enough to overtop the bank in the areas where channel depth is more than a meter. If the permeability of the silt/clay layer is low, then it is unlikely that the increase in WSE with the LW obstruction will increase lateral bank infiltration (Figure 22 & 23). This is because the water is unlikely to exceed the thickness of the silt/clay layer. As pointed out in the comparison of MP-1 and stream discharge, current annual high stream flows do not appear to cause aquifer recharge, as high GW levels frequently precede the peak in spring discharge (Figure 10 & 12).

Discussion Summary

The GW levels within the monitoring wells have not experienced significant change since their installation (Figures 10, 11, 12, & 13). The floodplain aquifer at Indian Creek is unlikely to store water into the late summer season because of the stratigraphy of the floodplain. The vertical movement of water within the floodplain aquifer is restricted by the zones of fine sediment and low permeability surrounding the ubiquitous sand and gravel layer. The GW levels in the monitoring wells are most likely not representative of the actual GW level. The rapid movement of water within the well pipes is most likely attributed to the low permeability of the fine sediment layers creating a pressurized push up the well once the sand and gravel layer has become saturated.

Water most likely flows into the floodplain from the hills, where the sandstone bedrock layer is near the surface, during snowmelt and rain fall. Figure 24 shows the fine

sediment silt/clay zone thins considerably towards the hill at the downstream well cluster. The thickness of the zone and distance to which it reaches the valley wall is unknown. The same goes for the gray clay zone, but it is possible the gray clay thins towards the hill as well and the sand and gravel from above and below the gray clay are nearly connected. For the instream wood to have a role in recharging the GW, much more water will need to find its way to the floodplain surface for a longer period.

CHAPTER V

CONCLUSIONS

This study assessed the short-term impact of instream large wood restoration on the recharge and storage of the floodplain aquifer at Indian Creek. The groundwater was evaluated using pressure transducer data, which begins prior to the wood restoration project. The stratigraphy of the floodplain was described at multiple sites throughout the project reach to investigate how the sediment affects the groundwater recharge and storage potential. Sediment grain-size analysis was performed to better understand the composition of the sediment and estimate porosity values within the floodplain. A streamflow model was run at various known discharges of Indian Creek to understand what changes the instream wood might have on the water surface elevation and floodplain inundation.

Groundwater levels were found to be unaffected by the presence of the instream large wood. Data from six groundwater monitoring wells showed no sustained increase to base levels or seasonal peaks after the emplacement of the large wood. The comparison of precipitation data and stream discharge with groundwater levels commonly show an annual pattern of high precipitation leading to high groundwater levels, with the peak stream discharge lagging behind the peak in groundwater levels. Groundwater levels are often in decline when the seasonal peak stream discharge occurs.

The stratigraphy of the floodplain aquifer at stream level and above contains five common zones. Notable in these zones is the amount of clay and silt found throughout much of the thickness of the floodplain. A silt zone and a silt/clay zone dominate the

upper 1.5 meter of the floodplain stratigraphy. Common throughout the stratigraphy below the silt/clay is a sand and gravel zone located at the stream level, often found as the stream bed. Below the sand and gravel zone is a zone of gray clay. The gray clay forms the bottom of the stream bed in many places. It has also been found throughout the floodplain.

Streamflow model results showed the addition of large wood to the existing stream channel is unlikely to cause a large change in flow depth that would increase the lateral movement of water into the floodplain aquifer. Model results also showed the addition of the instream wood does not greatly increase floodplain inundation or increase the chances of water to overtop streambanks that are more than a meter high.

The large wood restoration project at Indian Creek is still relatively recent and work is still being performed at the site. These results only suggest that the wood in the stream is yet to have an impact on the groundwater recharge and storage. Further investigation of the floodplain stratigraphy at the headwater tributaries of the Yakima River can provide a greater understanding of the regional effectiveness of instream large wood on groundwater recharge and storage.

REFERENCES

Boylan, N. C., 2019, Assessing the Link Between Large Wood Restoration and Groundwater Recharge and Storage: An Investigation of Indian Creek in Washington State.

DeKnikker, R., 2016, Teanaway Community Forest Aquatic Restoration Project 60% Design Report.

Díez, J.R., Larrańaga, S., Elosegi, A., and Pozo, J., 2000, Effect of removal of wood on streambed stability and retention of organic matter: Journal of the North American Benthological Society, v. 19, p. 621–632, doi:10.2307/1468121.

Dolloff, C.A., and Warren, M.L., 2003, Fish relationships with large wood in small streams: American Fisheries Society Symposium, v. 2003, p. 179–193.

Eddy, M.P., Umhoefer, P.J., Miller, R.B., Donaghy, E.E., Gundersen, M., and Senes, F.I., 2017, Sedimentary, volcanic, and structural processes during triple-junction migration: Insights from the Paleogene record in central Washington: GSA Field Guides, v. 49, p. 143–173, doi:10.1130/2017.0049(07).

Emmons, J.D., 2013, Quantifying the restorable water volume of Sierran meadows: ProQuest Dissertations and Theses, p. 67, http://193.60.48.5/docview/1526495137?accountid=15997%0Ahttp://resolver.ebscohost.com/openurl?ctx_ver=Z39.88-2004&ctx_enc=info:ofi/enc:UTF-8&rfr_id=info:sid/ProQuest+Dissertations+%26+Theses+A%26I&rft_val_fmt=info:ofi/fmt:kev:mtx:dissertation&rft.genre=diss.

Enefalk, Å., Watz, J., Greenberg, L., and Bergman, E., 2017, Winter sheltering by juvenile brown trout (Salmo trutta) – effects of stream wood and an instream ectothermic predator: Freshwater Biology, v. 62, p. 111–118, doi:10.1111/fwb.12854.

Fetherston, K.L., Naiman, R.J., and Bilby, R.E., 1995, Large woody debris, physical process, and riparian forest development in montane river networks of the Pacific Northwest: Geomorphology, v. 13, p. 133–144, doi:10.1016/0169-555X(95)00033-2.

Fox, M., and Bolton, S., 2007, A Regional and Geomorphic Reference for Quantities and Volumes of Instream Wood in Unmanaged Forested Basins of Washington State: North American Journal of Fisheries Management, v. 27, p. 342–359, doi:10.1577/m05-024.1.

Freeman, G. E., Copeland, R. R., Rahmeyer, W., & Derrick, D. L., 1998, Field determination of Manning's n value for shrubs and woody vegetation. In Engineering Approaches to Ecosystem Restoration (pp. 48-53).

Gurnell, A.M., and Sweet, R., 1998, The distribution of large woody debris accumulations and pools in relation to woodland stream management in a small, low-gradient stream: Earth Surface Processes and Landforms, v. 23, p. 1101–1121, doi:10.1002/(SICI)1096-9837(199812)23:12<1101::AID-ESP935>3.0.CO;2-O.

Huggenberger, P., and Aigner, T., 1999, Introduction to the special issue on aquifer-

sedimentology: Problems, perspectives and modern approaches: Sedimentary Geology, v. 129, p. 179–186, doi:10.1016/S0037-0738(99)00101-3.

Jackson, C.R., and Sturm, C.A., 2002, Woody debris and channel morphology in first- and second-order forested channels in Washington's coast ranges: Water Resources Research, v. 38, p. 16-1-16–14, doi:10.1029/2001wr001138.

Johnson, A. I., 1967, Specific yield: compilation of specific yields for various materials No. 1662, US Government Printing Office.

Jones, K.K., Anlauf-Dunn, K., Jacobsen, P.S., Strickland, M., Tennant, L., and Tippery, S.E., 2014, Effectiveness of Instream Wood Treatments to Restore Stream Complexity and Winter Rearing Habitat for Juvenile Coho Salmon: Transactions of the American Fisheries Society, v. 143, p. 334–345, doi:10.1080/00028487.2013.852623.

Mao, L., Ravazzolo, D., and Bertoldi, W., 2020, The role of vegetation and large wood on the topographic characteristics of braided river systems: Geomorphology, v. 367, p. 107299, doi:10.1016/j.geomorph.2020.107299.

Mellina, E., & Hinch, S. G. 2009, Influences of riparian logging and in-stream large wood removal on pool habitat and salmonid density and biomass: a meta-analysis. Canadian Journal of Forest Research, 39(7), 1280-1301.

Nagayama, S., Nakamura, F., Kawaguchi, Y., and Nakano, D., 2012, Effects of configuration of instream wood on autumn and winter habitat use by fish in a large remeandering reach: Hydrobiologia, v. 680, p. 159–170, doi:10.1007/s10750-011-0913-z.

Nash, C.S., Grant, G.E., Selker, J.S., and Wondzell, S.M., 2020, Discussion: "Meadow Restoration Increases Baseflow and Groundwater Storage in the Sierra Nevada Mountains of California" by Luke J.H. Hunt, Julie Fair, and Maxwell Odland: Journal of the American Water Resources Association, v. 56, p. 182–185, doi:10.1111/1752-1688.12796.

Redfield-Wilder, J., 2019, After 40 years, Acquavella adjudication is coming to close: Department of Ecology State of Washington, https://ecology.wa.gov/Blog/Posts/April-2019/After-40-years,-Acquavella-adjudication-is-coming (accessed 2021).

Reich, M., Kershner, J.L., and Wildman, R.C., 2003, Restoring Streams with Large Wood : A Synthesis: American Fisheries Society Symposium 37: International Conference on Wood in World Rivers, p. 355–366.

Richard, G., Cousin, I., Sillon, J.F., Bruand, A., and Guérif, J., 2001, Effect of compaction on the porosity of a silty soil: Influence on unsaturated hydraulic properties: European Journal of Soil Science, v. 52, p. 49–58, doi:10.1046/j.1365-2389.2001.00357.x.

Sawyer, A.H., and Cardenas, M.B., 2012, Effect of experimental wood addition on hyporheic exchange and thermal dynamics in a losing meadow stream: Water Resources Research, v. 48, p. 1–11, doi:10.1029/2011WR011776.

Schwartz, F. W., & Zhang, H., 2003, Fundamentals of Groundwater John Wiley & Sons. New York, 583.

Scott, D.N., Wohl, E., and Yochum, S.E., 2019, Wood Jam Dynamics Database and

Assessment Model (WooDDAM): A framework to measure and understand wood jam characteristics and dynamics: River Research and Applications, p. 1–12, doi:10.1002/rra.3481.

Swanson, F.J., Gregory, S. V., Sedell, J.R., and Campbell, A.G., 1982, Land-water interactions: the riparian zone.: Analysis of coniferous forest ecosystems in the western United States, p. 267–291.

Tabor, R.W., Frizzell, V.A., Vance, J.A., and Naeser, C.W., 1984, Ages and stratigraphy of lower and middle Tertiary sedimentary and volcanic rocks of the central Cascades, Washington: application to the tectonic history of the Straight Creek fault, USA.: Geological Society of America Bulletin, v. 95, p. 26–44, doi:10.1130/0016-7606(1984)95<26:AASOLA>2.0.CO;2.

Tague, C., Valentine, S., and Kotchen, M., 2008, Effect of geomorphic channel restoration on streamflow and groundwater in a snowmelt-dominated watershed: Water Resources Research, v. 44, p. 1–10, doi:10.1029/2007WR006418.

Tonina, D., and Buffington, J.M., 2009, Hyporheic exchange in mountain rivers I: Mechanics and environmental effects: Geography Compass, v. 3, p. 1063–1086, doi:10.1111/j.1749-8198.2009.00226.x.

WDFW Public Affairs Office, 2017, Teanaway Community Forest: https://www.dnr.wa.gov/publications/amp_rec_tcf_map2015.pdf

Wohl, E., 2014, A legacy of absence: Wood removal in US rivers: Progress in Physical Geography, v. 38, p. 637–663, doi:10.1177/0309133314548091.

Wohl, E., 2013, Floodplains and wood: Earth-Science Reviews, v. 123, p. 194–212,

doi:10.1016/j.earscirev.2013.04.009.

APPENDIXES

APPENDIX A

Groundwater

Table A1. Manual measurements from the six groundwater monitoring wells used for this study. Measurements are depth to water in feet below the top of the well pipe.

Date	MP-1	MP-2	MP-3	MP-4	MP-5	MP-6
10/8/2018	Dry	6.39	3.98	7.95	5.91	5
10/26/2018	Dry	4.98	4.41	6.22	5.69	5.2
4/4/2019	4.80	1.75	2.49	5.37	3.29	3.61
6/28/2020	Dry	5.82	3.91	7.85	6.07	5.19
8/26/2020	Dry	6.10	4.41	8.22	6.35	5.61
10/21/2020	Dry	5.71	3.16	7.5	6.07	5.15
4/11/2021	5.90	3.56	2.91	5.64	3.51	3.65
4/28/2021	6.44	5.01	2.92	5.95	4.92	3.78
5/9/2021	6.67	5.19	3.12	6.48	5.14	4.1
5/29/2021	6.74	5.57	3.48	7.19	6.08	4.71
6/10/2021	Dry	5.65	3.67	7.48	6.1	4.92
10/31/2021	Dry	5.54			5.97	
11/7/2021			3.65	9.3		4.7

APPENDIX B

Stratigraphy

Table B1. Stratigraphic descriptions of the three sites at section 1 near the downstream well cluster (Figure 5B).

Section	Site	Zone	Depth (cm)	Description
1	1	1	0-42	Dark brown silt with some fine sand. Darker soil with 0.5 cm hard peds at top 15 cm. Approximately 1 cm gravel mixed in from 36-42 cm. Lower contact is sharp. Less than 1 cm, planar to wavy. Crumbly when dry. Dense roots in upper 30 cm. Color 10YR 3/3
		2	42-52	Silty clay. Medium brown with slight hits of red. Massive, no soil peds. Very few gravels. Lower contact 1-2 cm boundary, sharp change to no gravel. Color 7.5YR 3/3
		3	52-87	Gravel-clay-silt. Medium brown, little reddish. Gravel up to 3 cm. 1-2 cm common. No clear bedding. Lower contact ~1 m boundary, sharp change to no gravel. Color7.5 YR 4/4
		4	87-17	Mottled red and gray clay. Vertical red oxided rhizosphere with gray mottled clay mixed in. Gray slightly increses with depth. Just to the left of the section is a gravel lense with cobbles up to 5 cm. Color 7.5 YR 4/6
		5	170-200	Sandy with clay. Small gravels. Not dense with gravel. Pebbles are generally less than 1 cm. Color 5 YR 5/8
		6	200-220	Solid gray clay. Color 5 YR 6/1
1	2	1	0-25	Dark brown silty soil
			25-140	Medium brown silt
			140-180	Upper limit of gray clay nodules in red oxidized silt. Few gray nodules. At 147 cm, gray clay nodules increase with black vegetation organics.
			180-183	Sand and gravel in clay/silt matrix. Rounded gravel up to 5 cm.
1	3	1	0-30	Dark brown silt granular soil
		2	30-100	Med brown silt
		3	100-107	Red sand, gravel, clay. Very sticky. Rounded gravel <4cm.

Table B2. Stratigraphic descriptions of the stream bank at section 2, site 1 (Figure 5B). 2-1 is the only from this section.

Section	Site	Zone	Depth (cm)	Description
2	1	1	0-25	Light brown silty soil. Peds <0.5 cm that crumble easily. Long roots extend beyond 25 cm contact. Lower contact is sharp with dense gravels ~2 cm. Color Light brown 7.5 YR 4/6
		2	25-55	Gravel, silt, clay. Ped sizes 0.5-1.0 cm. Gravels are rounded, average ~1.0 cm. Some gravels up to 4 cm. Lower contact is gradual and wavy. Gravel size increases near contact. Color orange-red 5 YR 3/3.
		3	55-65	Silt and sand. Rounded rocks from 3-10 cm are densely distributed. Lower contact is gradual over 3 cm and rock size decreases.
		4	65-105	Clay with silt and little sand. Medium brown and red with oxidized rhizospheres throughout.
		5	105-135	Gray clay with oxidized rhizosphere. Charcoal within clumps of clay. Lower contact has small gravels within the clay. Contact transition ~2 cm.
		6	135-144	Dark gray clay with pebbles up to 3 cm. Pebbles are oxidized reddish-brown color. Pebbles size and abundance increases near the lower contact. Lower contact is a sharp change from dark gray to red and reddish-brown.
		7	144-190	Clay, silt, sand with

Table B3. Stratigraphic descriptions of the two sites at section 3 (Figure 5C).

Section	Site	Zone	Depth (cm)	Description
3	1	1	0-22	Dark brown-gray soil. Dense roots from abundant surface vegetation. Pebbles of 2-3 cm are common. Lower contact is blended and identified by an increase the abundance of pebbles.
		2	22-50	Light to dark brown sand and silt. Rounded and flat rounded pebbles up to 7 cm are abundant. Color changes to a gray hue at 28 cm, but composition remains consistent. Lower contact is sharp change.
		3	50-130	Orange-brown-gray silty clay. At 119 cm the color turns to gray with orange oxidized rhizosphere. Lower contact transitions abruptly with the presence of large cobbles and sand.
		4	130-156	Large cobbles over 10cm. Sandy clay matrix of orange-brown color. Lower contact turns to clay over 4-5 cm, cobbles disappear.
		5	156-170	Reddish-brown clay. Few pebbles and some gray coloration. Lower contact is a sharp transition.
		6	170-199	Blue-gray clay. Few small pebbles, abundance decreases with depth. Clay becomes purer. Lower contact occurs over 2 cm.
		7	199-below	Pebbles 3-5 cm in brown sand. Completely saturated.
	2	1	0-25	Vegetation and soil
		2	25-60	Silt, sand, clay with large cobbles ranging from 1 to 14 cm. Matrix become sand rich at 42 cm. At 50 cm, clay increases and the color turns to reddish-brown. Lower contact is gradual with clay increasing with depth. One large cobble removed was lower contact.
		3	60-84	Reddish-brown moist clay, still full of cobbles. Lower contact is an abrupt change to gray sand.
		4	84-120	Gray sand at the beginning. Auger went through a large log until 120 cm.
		5	120-140	Gray sand with some pebbles 1-4 cm. Filled

				with groundwater.

Table B4. Stratigraphic description of section 4 (Figure 5C).

Section	Site	Zone	Depth (cm)	Description
4	1	1	0-30	Soil with heavy vegetation
		2	30-37	Soil and clay mixture. Possibly mixed because of the auger.
		3	37-70	Pure gray clay to 70 cm where the auger stopped.

Table B5. Stratigraphic descriptions of the two sites at section 5 (Figure 5D).

Section	Site	Zone	Depth (cm)	Description
5	1	1	0-40	Silty clay. Dominant clay could have mix of surface sediments and influence of human activity. Site is on the slope of a canal.
		2	40-130	Brown and dark brown clay. Pure and high plasticity. Becomes stickier at 100 cm. Very moist at 110 cm. Water just below clay at 110 cm.
		3	130-140	Gravel, sand, clay mixed with water.
	2	1	0-27	Soil
		2	27-59	Medium brown silty clay. Becomes more clay rich with depth. Lower contact changes to gray clay at 59 cm. Sharp change in color.
		3	59-90	Gray clay. At 85 cm the clay becomes a deeper gray and is wet.
		4	90-100	Sand and cobbles. Very wet.
		5	100-129	Blue-gray wet clay. Some pebbles at top from transition. Groundwater fills at 129 cm.

APPENDIX C

Sediment Grain-Size Analysis

Table C1. Sediment values used for the Mastersizer analysis.

Unit	Total mass	Mass >0.5mm	Mass <0.5mm	Mass used (g)
1	14.582	6.8505	7.7315	0.13
2	20.482	6.5373	13.9447	0.121
3	23.037	12.2789	10.7581	0.128
4	66.624	48.2888	18.3352	0.119
5	50.904	8.408	42.496	0.116
6	8.604	0	8.604	0.107
7	45.4	12.5743	32.8257	0.117
8	39.512	27.1724	12.3396	0.113
9	13.456	0.2805	13.1755	0.101

Table C2. Sieve data from site 1-1.

Sample	Depth (cm)	Mass (g)	4mm	2mm	1mm	0.5mm	0.25mm	0.125mm	0.063mm	0.045mm	0.032mm	<0.032mm
1	5-7	14.5824	0	0.8968	2.2453	3.7084	3.2788	2.5435	1.4321	0.4775	N/A	N/A
2	34-37	20.4817	0	0.6393	0.1147	5.7833	4.839	3.4549	2.6448	1.0484	0.7244	1.2329
3	43-47	23.0368	0	0.9675	4.4301	6.8813	4.8955	2.8136	1.6316	0.3698	0.3949	0.1566
4	60-68	66.236	13.5637	8.6093	8.3032	17.813	9.7427	4.3796	2.3433	0.4788	0.4472	0.196
5	99-102	50.9039	0.1045	0.4125	5.8901	2.0009	15.7844	11.214	7.9556	3.2056	2.1824	1.3441
6	144	8.604	0	0	0	0	2.8361	2.1026	2.597	0.7716	0.2327	0.064
7	140-150	45.4001	0	0.3679	0.3875	11.819	15.5535	8.0858	5.3295	1.495	1.7757	1.1689
8	185-190	39.5115	5.2409	5.6447	7.7415	8.5453	5.5748	2.946	1.8394	0.7048	0.5992	0.3458
9	230-240	13.4561	0	0	0.0463	0.2342	1.8339	4.0774	5.2318	1.9698	0.04264	0.0201

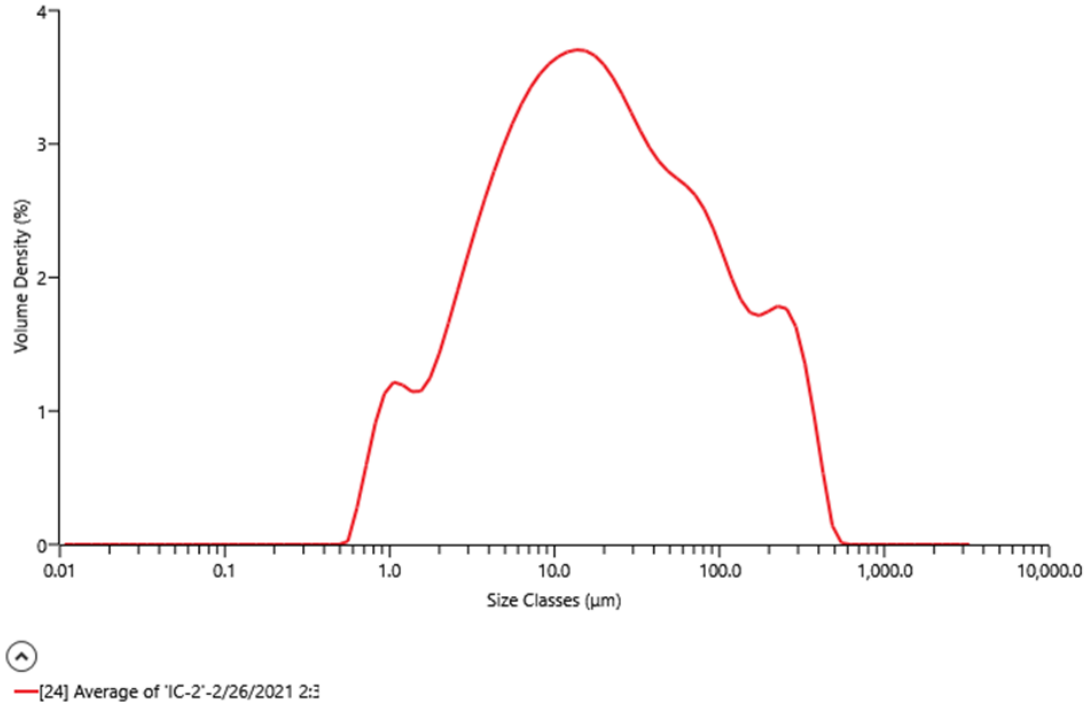

Figure C1. Mastersizer data of unit 2 from site 1-1 graphed.

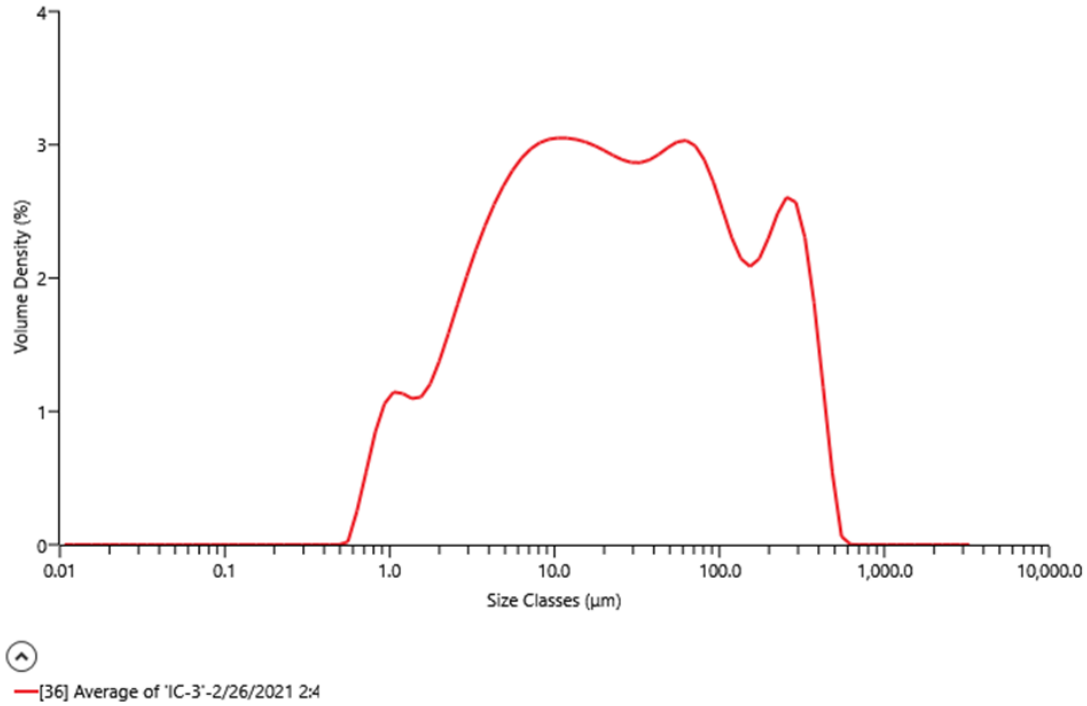

Figure C2. Mastersizer data of unit 3 from site 1-1 graphed.

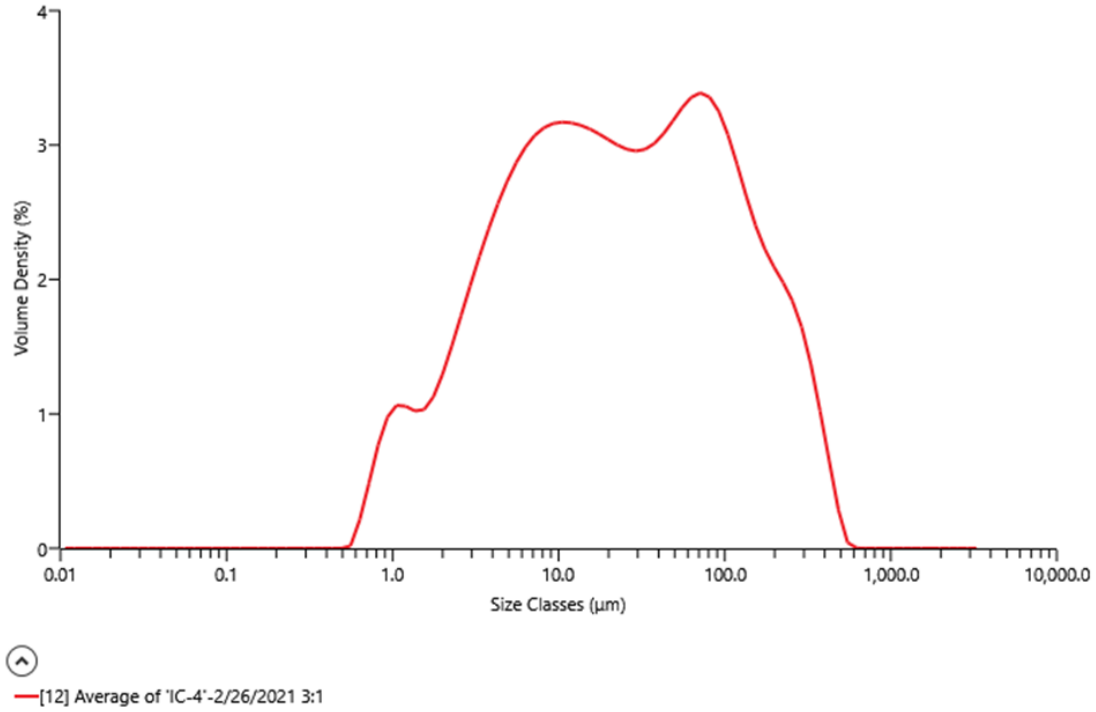

Figure C3. Mastersizer data of unit 4 from site 1-1 graphed.

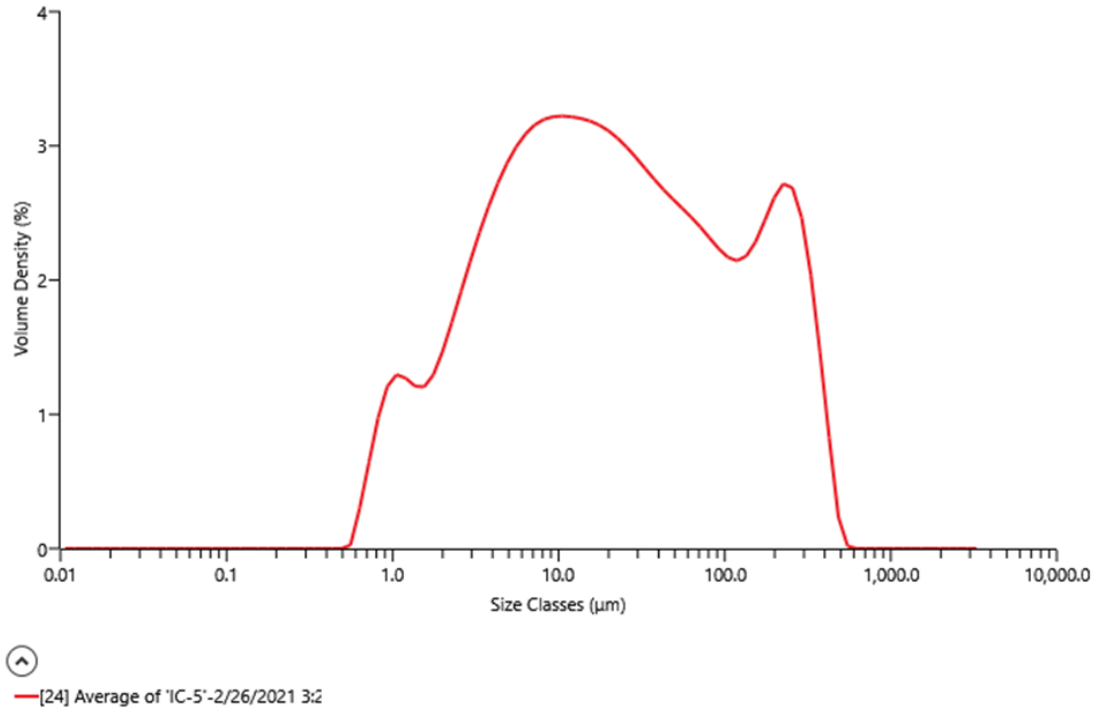

Figure C4. Mastersizer data of unit 5 from site 1-1 graphed.

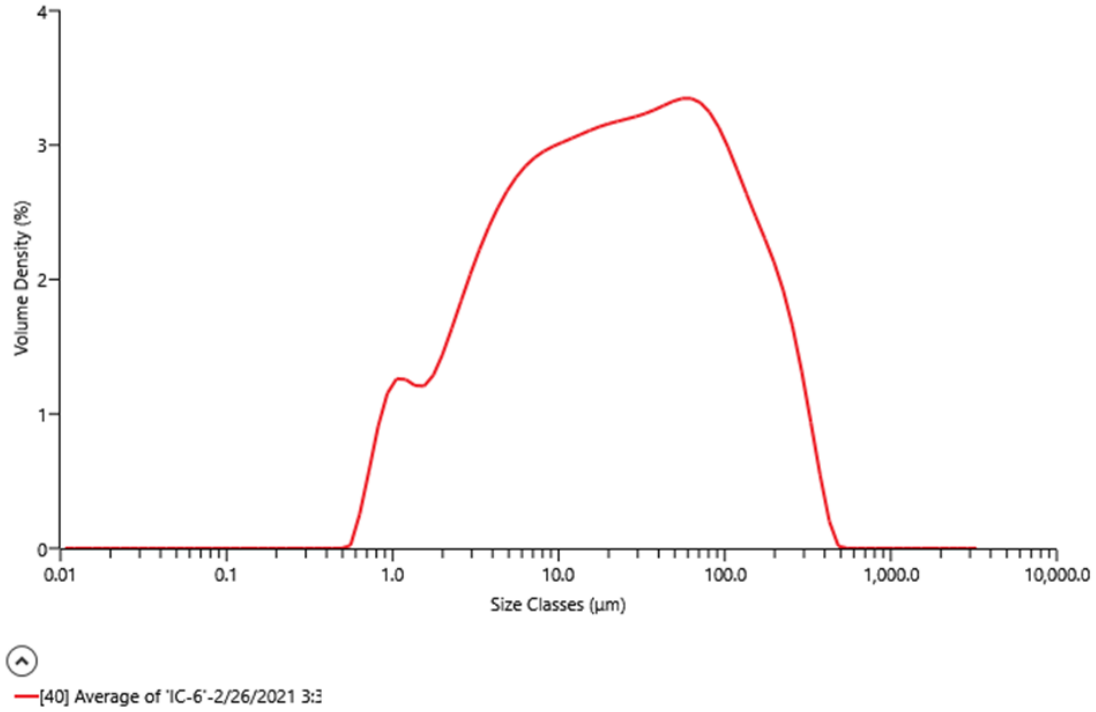

Figure C5. Mastersizer data of unit 6 from site 1-1 graphed.

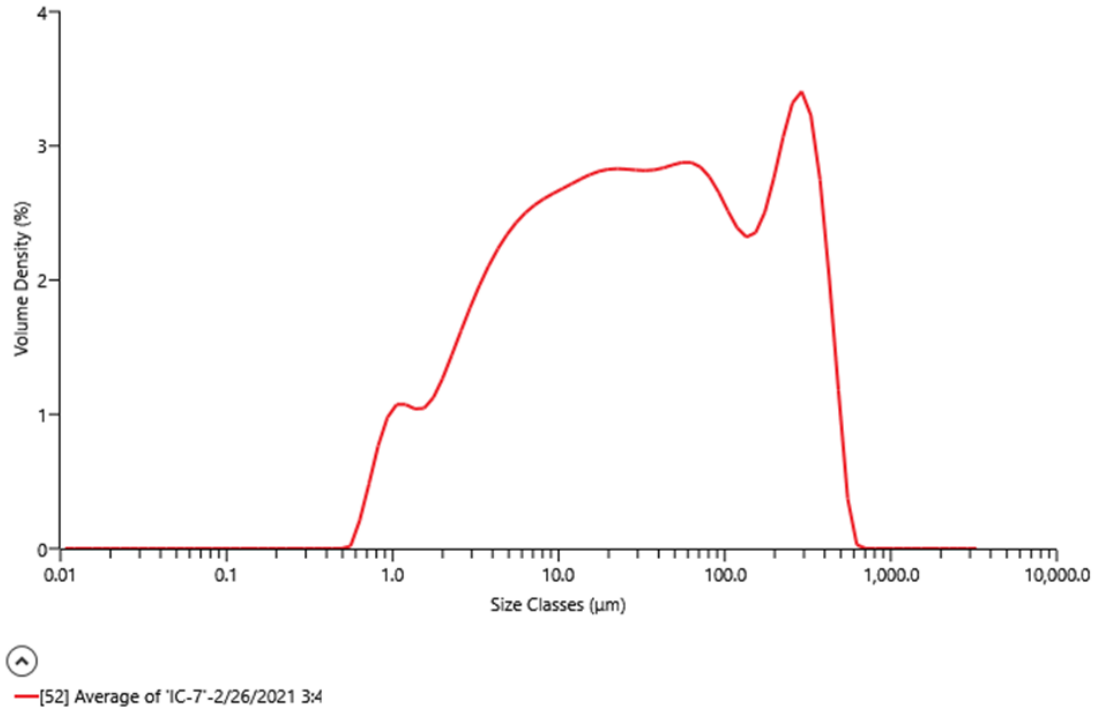

Figure C6. Mastersizer data of unit 7 from site 1-1 graphed.

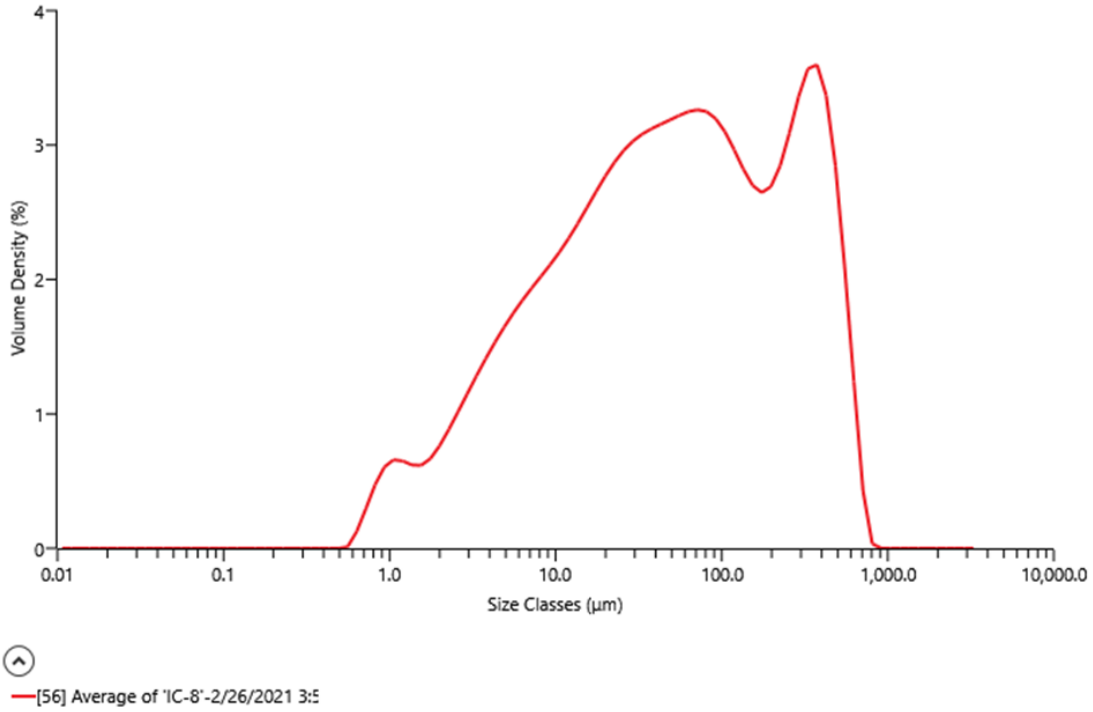

Figure C7. Mastersizer data of unit 8 from site 1-1 graphed.

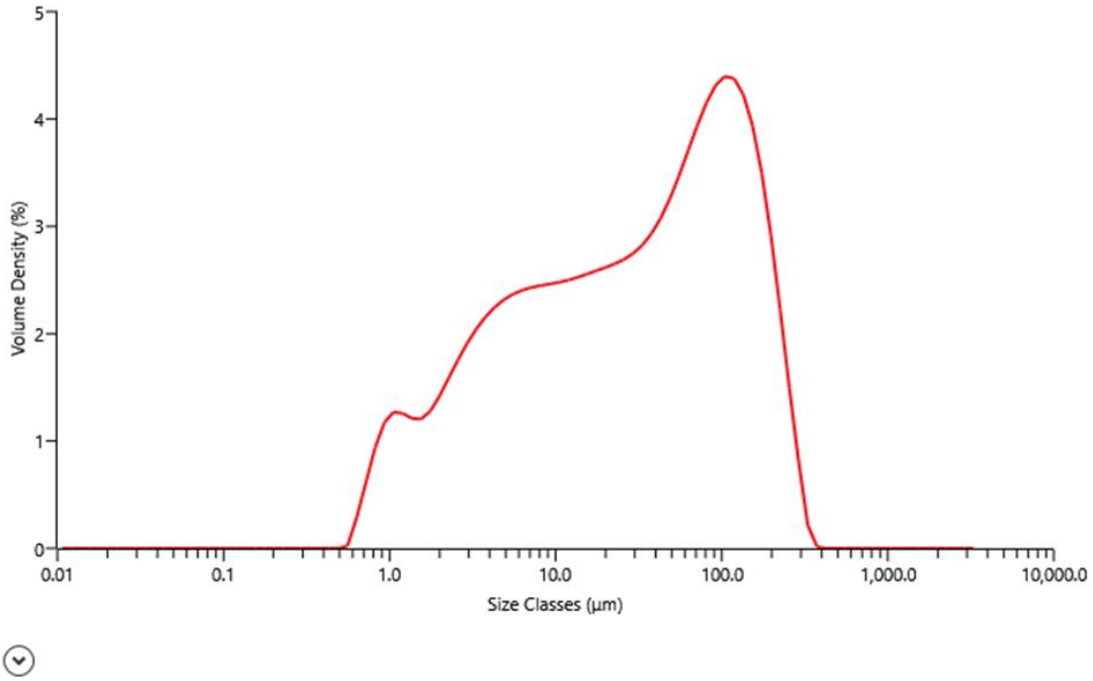

Figure C8. Mastersizer data of unit 9 from site 1-1 graphed.

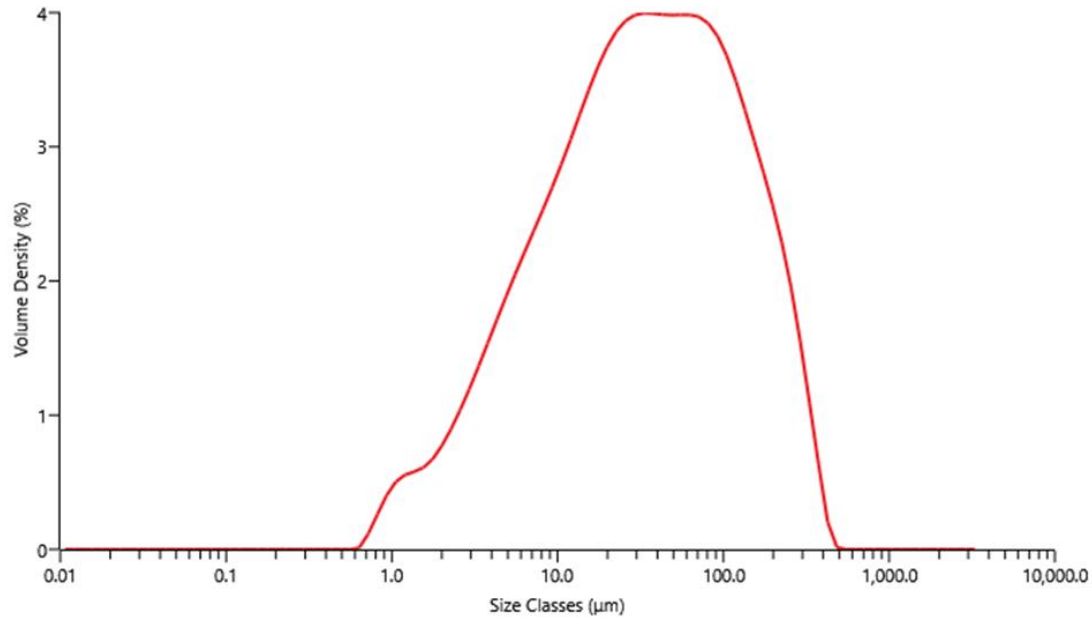

Figure C9. Mastersizer data from the gray clay sample from the North Fork Teanaway River graphed.

APPENDIX D

Stream Model

Table D1. Stream model results of the 6 ft^3/s without instream obstructions.

Discharge	Min CH el	W.S. El	Crit w.s.	e.g elev	e.g. slope	vel chnl	Flow area	top width	Froude
6	2499.36	2499.85		2499.95	0.011035	2.51	2.39	7.02	0.76
6	2497.94	2498.34	2498.34	2498.47	0.020636	2.89	2.08	7.96	1
6	2495.58	2496.05	2496.01	2496.15	0.013704	2.52	2.38	8.19	0.83
6	2493.86	2494.37	2494.37	2494.52	0.019709	3.18	1.89	5.98	1
6	2491.74	2492.21	2492.21	2492.36	0.020146	3.05	1.97	6.83	1
6	2489.51	2489.94	2489.94	2490.08	0.020007	3.02	1.99	6.94	1
6	2487.13	2487.7	2487.69	2487.86	0.019094	3.2	1.88	5.74	0.99
6	2485.91	2486.52	2486.41	2486.61	0.008608	2.4	2.5	6.43	0.68
6	2484.85	2485.28	2485.26	2485.4	0.017554	2.83	2.12	7.4	0.93
6	2483.85	2484.34		2484.4	0.006341	1.95	3.08	8.77	0.58
6	2482.9	2483.53		2483.64	0.009375	2.59	2.32	5.64	0.71
6	2482.15	2482.62	2482.54	2482.7	0.009192	2.22	2.7	8.34	0.69
6	2480.94	2481.21	2481.21	2481.3	0.023235	2.46	2.44	12.99	1

Table D2. Stream model results of the 6 ft^3/s with instream obstructions.

Discharge	Min CH el	W.S. El	Crit w.s.	e.g. elev	e.g. slope	vel chnl	Flow area	top width	Froude
6	2499.36	2500.5		2500.54	0.012722	1.46	4.12	5.19	0.29
6	2497.94	2498.57		2498.65	0.030795	2.23	2.69	5.71	0.57
6	2495.58	2496.65		2496.68	0.013448	1.5	4	5.91	0.32
6	2493.86	2494.94		2495	0.021244	2.04	2.95	4.17	0.43
6	2491.74	2492.68		2492.71	0.024738	1.51	3.96	6.93	0.35
6	2489.51	2490.33		2490.38	0.021981	1.74	3.45	5.92	0.4
6	2487.27	2488.41		2488.45	0.017024	1.63	3.68	5.55	0.35
6	2485.91	2487.02		2487.05	0.011703	1.34	4.48	6.36	0.28
6	2484.85	2485.79		2485.81	0.013064	1.32	4.55	7.1	0.29
6	2483.85	2484.87		2484.88	0.007035	1.04	5.79	7.65	0.21
6	2482.9	2484.04		2484.07	0.009474	1.49	4.02	4.4	0.28
6	2482.15	2483.01	2482.62	2483.03	0.011435	1.19	5.06	11.43	0.31
6	2480.94	2481.3	2481.21	2481.34	0.026899	1.6	3.75	14.87	0.56

Table D3. Stream model results of the 13.4 ft^3/s without instream obstructions.

Discharge	Min CH el	W.S. El	Crit w.s.	e.g. elev	e.g. slope	vel chnl	Flow area	top width	Froude
13.4	2499.36	2500.07	2500.01	2500.24	0.012712	3.31	4.04	8.68	0.86
13.4	2497.94	2498.54	2498.54	2498.73	0.018116	3.54	3.78	9.65	1
13.4	2495.58	2496.24	2496.2	2496.41	0.014049	3.3	4.06	9.52	0.89
13.4	2493.86	2494.59	2494.59	2494.84	0.017756	3.95	3.39	7.11	1.01
13.4	2491.74	2492.42	2492.42	2492.64	0.01836	3.76	3.57	8.38	1.02
13.4	2489.51	2490.15	2490.15	2490.36	0.018255	3.68	3.64	8.81	1.01
13.4	2487.13	2487.93	2487.93	2488.18	0.017801	3.97	3.38	7.05	1.01
13.4	2485.91	2486.77	2486.65	2486.92	0.009061	3.12	4.29	7.67	0.74
13.4	2484.85	2485.47	2485.47	2485.68	0.017814	3.69	3.64	8.58	1
13.4	2483.85	2484.6		2484.69	0.005438	2.39	5.6	10.37	0.57
13.4	2482.9	2483.81	2483.69	2483.98	0.009682	3.33	4.03	6.79	0.76
13.4	2482.15	2482.84	2482.75	2482.96	0.01049	2.74	4.89	11.92	0.75
13.4	2480.94	2481.36	2481.36	2481.49	0.021683	2.88	4.65	18.38	1.01

Table D4. Stream model results of the 13.4 ft^3/s with instream obstructions.

Discharge	Min CH el	W.S. El	Crit w.s.	e.g. elev	e.g. slope	vel chnl	Flow area	top width	Froude
13.4	2499.36	2501.04		2501.09	0.015313	1.79	7.48	7.55	0.32
13.4	2497.94	2499.01		2499.1	0.026849	2.44	5.49	7.75	0.51
13.4	2495.58	2497.2		2497.24	0.013452	1.76	7.61	7.2	0.3
13.4	2493.86	2495.47		2495.55	0.022218	2.31	5.8	6.56	0.43
13.4	2491.74	2493.15		2493.2	0.024877	1.75	7.64	8.18	0.32
13.4	2489.51	2490.84		2490.9	0.021232	1.94	6.92	7.66	0.36
13.4	2487.27	2488.97		2489.02	0.016808	1.86	7.2	7	0.32
13.4	2485.91	2487.58		2487.61	0.011837	1.57	8.55	8.09	0.27
13.4	2484.85	2486.33		2486.36	0.013327	1.54	8.69	8.44	0.27
13.4	2483.85	2485.52		2485.54	0.005522	1	13.35	15.86	0.19
13.4	2482.9	2484.64		2484.7	0.014187	1.9	7.05	5.56	0.3
13.4	2482.15	2483.31	2482.86	2483.34	0.012743	1.4	9.59	18.67	0.34
13.4	2480.94	2481.49	2481.36	2481.54	0.026929	1.75	7.65	26.38	0.57

Table D5. Stream model results of the 15.9 ft^3/s without instream obstructions.

Discharge	Min CH el	W.S. El	Crit w.s.	e.g. elev	e.g. slope	vel chnl	Flow area	top width	Froude
15.9	2499.36	2500.12	2500.07	2500.31	0.012993	3.49	4.55	9.18	0.87
15.9	2497.94	2498.59	2498.59	2498.8	0.017898	3.71	4.28	10.07	1
15.9	2495.58	2496.3	2496.26	2496.48	0.013837	3.46	4.6	9.9	0.9
15.9	2493.86	2494.66	2494.66	2494.92	0.01748	4.15	3.83	7.37	1.01
15.9	2491.74	2492.48	2492.48	2492.72	0.017493	3.89	4.09	8.8	1
15.9	2489.51	2490.21	2490.21	2490.44	0.01736	3.79	4.2	9.35	1
15.9	2487.13	2488	2488	2488.26	0.017269	4.12	3.86	7.41	1.01
15.9	2485.91	2486.83	2486.71	2487	0.009255	3.31	4.8	7.95	0.75
15.9	2484.85	2485.52	2485.52	2485.75	0.017578	3.87	4.11	8.92	1
15.9	2483.85	2484.67		2484.77	0.005319	2.51	6.34	10.76	0.58
15.9	2482.9	2483.89	2483.76	2484.08	0.009472	3.47	4.58	7.12	0.76
15.9	2482.15	2482.89	2482.8	2483.02	0.011326	2.9	5.49	13.01	0.79
15.9	2480.94	2481.4	2481.4	2481.53	0.020617	2.93	5.43	20.18	1

Table D6. Stream model results of the 15.9 ft^3/s with instream obstructions.

Discharge	Min CH el	W.S. El	Crit w.s.	e.g. elev	e.g. slope	vel chnl	Flow area	top width	Froude
15.9	2499.36	2501.16		2501.22	0.01612	1.9	8.37	7.98	0.33
15.9	2497.94	2499.14		2499.23	0.02494	2.44	6.53	8.45	0.49
15.9	2495.58	2497.35		2497.4	0.013832	1.81	8.77	7.95	0.3
15.9	2493.86	2495.6		2495.69	0.021666	2.37	6.7	6.92	0.43
15.9	2491.74	2493.29		2493.34	0.025283	1.8	8.83	8.63	0.31
15.9	2489.51	2490.99		2491.05	0.020974	1.97	8.08	8.12	0.35
15.9	2487.27	2489.12		2489.17	0.016972	1.92	8.28	7.32	0.32
15.9	2485.91	2487.74		2487.78	0.011591	1.61	9.89	8.41	0.26
15.9	2484.85	2486.45		2486.49	0.014355	1.63	9.75	8.87	0.27
15.9	2483.85	2485.68		2485.7	0.004961	1	15.9	17.16	0.18
15.9	2482.9	2484.83		2484.89	0.015124	1.95	8.16	6.3	0.3
15.9	2482.15	2483.42	2482.93	2483.45	0.013554	1.29	12.3	31.31	0.36
15.9	2480.94	2481.53	2481.4	2481.58	0.026881	1.82	8.74	28.24	0.58

Table D7. Stream model results of the 36.4 ft^3/s without instream obstructions.

Discharge	Min CH el	W.S. El	Crit w.s.	e.g. elev	e.g. slope	vel chnl	Flow area	top width	Froude
36.4	2499.36	2500.44	2500.43	2500.79	0.014896	4.76	7.65	10.65	0.99
36.4	2497.94	2498.91	2498.91	2499.24	0.016048	4.59	7.93	12.47	1.01
36.4	2495.58	2496.62	2496.6	2496.93	0.014017	4.45	8.19	12.17	0.96
36.4	2493.86	2495.06	2495.06	2495.46	0.01539	5.05	7.21	9.27	1.01
36.4	2491.74	2492.84	2492.84	2493.19	0.015587	4.78	7.62	10.95	1.01
36.4	2489.51	2490.55	2490.55	2490.9	0.015742	4.72	7.72	11.42	1.01
36.4	2487.13	2488.41	2488.4	2488.79	0.014637	4.96	7.35	9.35	0.99
36.4	2485.91	2487.22	2487.11	2487.53	0.010774	4.46	8.15	9.56	0.85
36.4	2484.85	2485.87	2485.87	2486.23	0.015568	4.8	7.58	10.79	1.01
36.4	2483.85	2485.21		2485.33	0.004494	2.81	12.95	16.23	0.55
36.4	2482.9	2484.29	2484.2	2484.63	0.011198	4.68	7.78	8.63	0.87
36.4	2482.15	2483.18	2483.12	2483.37	0.013373	3.51	10.37	20.79	0.88
36.4	2480.94	2481.6	2481.6	2481.77	0.019405	3.34	10.91	31.87	1

Table D8. Stream model results of the 36.4 ft^3/s with instream obstructions.

Discharge	Min CH el	W.S. El	Crit w.s.	e.g. elev	e.g. slope	vel chnl	Flow area	top width	Froude
36.4	2499.36	2501.73		2501.81	0.016688	2.24	16.22	16.07	0.39
36.4	2497.94	2499.91		2500.01	0.019355	2.59	14.05	10.9	0.4
36.4	2495.58	2498.33		2498.4	0.013482	2.04	17.83	9.88	0.27
36.4	2493.86	2496.6		2496.67	0.022854	2.13	17.11	27.21	0.47
36.4	2491.74	2494.18		2494.24	0.025883	2.02	18	13.74	0.31
36.4	2489.51	2491.96		2492.02	0.019134	2.01	18.09	13.73	0.31
36.4	2487.27	2490.21		2490.28	0.016092	2.06	17.65	10.86	0.29
36.4	2485.91	2488.77		2488.83	0.013105	1.91	19.03	9.97	0.24
36.4	2484.85	2487.23		2487.29	0.018179	2.07	17.61	11.27	0.29
36.4	2483.85	2486.48		2486.5	0.004275	1.09	33.27	26.89	0.17
36.4	2482.9	2485.57		2485.62	0.027153	1.85	19.63	47.49	0.51
36.4	2482.15	2483.69	2483.27	2483.73	0.014004	1.58	23.03	45.65	0.39
36.4	2480.94	2481.76	2481.6	2481.84	0.026899	2.31	15.76	34.17	0.6